Summer 2006

Fabrication of hydroxyapatite-biodegradable polymer scaffolds by electrospinning for potential bone tissue application

Satomi Suzuki
New Jersey Institute of Technology

ABSTRACT

FABRICATION OF HYDROXYAPATITE-BIODEGRADABLE POLYMER SCAFFOLDS BY ELECTROSPINNING FOR POTENTIAL BONE TISSUE APPLICATION

by
Satomi Suzuki

The purpose of this study is to determine the potential of combining hydroxyapatite (HA) and polymers to form synthetic composite materials used for bone tissue engineering applications. In this study, ceramic-biodegradable polymer composites are fabricated by electrospinning method. The biodegradable polymers used are poly(L-lactic acid) (PLLA), and poly(lactide-*co*-glycolide) (PLGA). Two types of HA-polymer solutions are first prepared to achieve HA weight percentage of 0, 10, and 25% of the total combined weight of HA and PLLA, and HA and PLGA. The solutions are electrospun to form nanofibrous mats incorporated with HA powder. A biomimetic process was also conducted as a secondary approach.

The nanofibrous mats obtained follow characterization using scanning electron microscope (SEM) - Energy Dispersive X-ray Analysis (EDXA), Thermogravimetric Analysis (TGA), and X-ray Diffraction (XRD). In this study, hydroxyapatite (HA) particles were successfully incorporated into the three dimensional porous biodegradable PLLA and PLGA polymer fiber mats by electrospinning.

FABRICATION OF HYDROXYAPATITE-BIODEGRADABLE POLYMER SCAFFOLDS BY ELECTROSPINNING FOR POTENTIAL BONE TISSUE APPLICATION

by
Satomi Suzuki

A Thesis
Submitted to the Faculty of
New Jersey Institute of Technology
in Partial Fulfillment of the Requirements for the Degree of
Master of Science in Biomedical Engineering

Department of Biomedical Engineering

August 2006

APPROVAL PAGE

FABRICATION OF HYDROXYAPATITE-BIODEGRADABLE POLYMER SCAFFOLDS BY ELECTROSPINNING FOR POTENTIAL BONE TISSUE APPLICATION

Satomi Suzuki

Dr. Treena L Arinzeh, Thesis Advisor — Date
Assistant Professor of Biomedical Engineering, NJIT

Dr. Michael Jaffe, Committee Member — Date
Professor of Biomedical Engineering, NJIT

Dr. George Collins, Committee Member — Date
Research Professor of Biomedical Engineering, NJIT

BIOGRAPHICAL SKETCH

Author: Satomi Suzuki

Degree: Master of Science

Date: May 2006

Undergraduate and Graduate Education:

- Master of Science in Biomedical Engineering,
  New Jersey Institute of Technology, Newark, NJ, 2006

- Bachelor of Science in Biology,
  William Paterson University of New Jersey, Wayne, NJ, 2002

Major: Biomedical Engineering

Achieving is a great feeling,
Achieving while being Myasthenia Gravis patient
is an indescribable feeling.

To my beloved family in Japan

長い留学生活を支えてくれた
両親と兄に感謝の気持ちをこめて

ACKNOWLEDGMENT

I would like to express my appreciation to Dr. Treena Arinzeh, my research advisor, for her support and encouragement. She provided me valuable and countless resources and gave me guidance throughout the research work. I would also like to thank Dr. Michael Jaffe and Dr. George Collins for actively participating in my committee. Dr. Roumiana Petrova's help for the sample evaluation with X-ray Diffraction analysis is also greatly appreciated.

Special thanks are given to Shobana Shanmugasundaram for helping and guiding me all through the research work. I learned not only the technical and academic skills, but also how to face the unexpected problems and to evaluate the importance of the research work from her.

I would also like to thank my family members in Japan for giving me a chance to study abroad. All the support and encouragement they have given to me are greatly appreciated. Hachi, my best friend who encouraged me through the research work, is also deserving of recognition for her support.

TABLE OF CONTENTS

TABLE OF CONTENTS
(Continued)

Chapter **Page**

LIST OF TABLES

LIST OF FIGURES

LIST OF FIGURES
(Continued)

CHAPTER 1

INTRODUCTION

In orthopedics, defects in large bones have been a major problem. The need for bone regeneration to heal bone diseases caused by bone tumors, bone infection, and bone loss by trauma is growing; however, no optimal solution has been established yet for the repair of large bone defects of greater than 3 cm [1, 2]. Bone grafts have played a major role in therapies for bone defects. In the United States, more than 300,000 bone graftings were conducted in 1998 [3]. The number of procedures conducted increased to 500,000 in 1999 and the estimated cost for these bone-grafting procedures approaches $2.5 billion per year [3]. The graft transplanting using autologous or allogenic bone grafts has been applied as one of the traditional treatments for the bone repair with nine out of ten of procedures in 1998 involved either autograft or allograft [3, 4].

The autograft is the bone graft in which tissue is harvested from the patient and placed at the injury site. This is an ideal bone graft because it has all the characteristics required for new bone growth; however, the additional surgery required to harvest the autograft increases the possibility of complications such as infection, inflammation, and chronic pain. Quantities of the bone tissue to be harvested are also limited and may result in supply shortage. The allograft is another bone graft procedure in which tissue to be harvested and placed at the injury site is taken from donors or cadavers. Allografts eliminate some shortcomings of autograft bone implants such as morbidity of donor site and problems with limited supply. However, due to the use of non-self tissue, allografts always carry risks of disease transmission and immunorejection by patients. In 1992, one

case of hepatitis B and three cases of hepatitis C transmission associated with allografts have been reported [3]. In 2000, two patients received allografts developed septic arthritis, and in 2001 one patient died from clostridium sordellii infection within four days of allograft surgery [3]. After this, 25 more cases of infection or illness related with allografts were revealed by the investigation of the Centers for Disease Control and Prevention [3].

The shortcomings and limitations associated with autografts and allografts accelerate the necessity of the development of alternatives that satisfy two criteria for a successful graft; osteoconduction and osteoinduction. Tissue engineering approach for bone repairing has been proposed as one of the alternatives. In tissue engineering, bioceramic scaffolds, osteogenic cells, growth factors, and physical forces play a role to repair bone defects [4].

Researchers have been devoted to bone tissue engineering where they develop three dimensional porous scaffolds with tissue-inducing factors [5]. The three dimensional porous scaffolds need to be designed so that they play an important role to manipulate osteoblasts functions and to guide and induce new bone formation. Materials used in scaffolds also need to be osteoconductive for osteoprogenitor cells to migrate and adhere onto the scaffolds, differentiate and form a new bone [6, 7]. The desirable scaffolds should be also biodegradable with proper degradation rate so that the scaffolds will eventually be replaced by newly formed bone. Thus the scaffold in bone tissue engineering should satisfy the requirements: biocompatiblility, osteoconductivity, interconnected porous structure, proper biodegradability, and proper mechanical strength.

Current study indicates that ceramics shows exceptional biocompatibility properties interacting bone cells and tissues and carries a great potential for bone tissue engineering application [8, 9]. The long-term direct osteointegration, the structural and functional connection between bone tissues and the implants, however, is not achieved by the osteoblasts adhesion to the ceramics surface alone [8]. Also, dense hydroxyapatite is not suitable for long term load bearing applications due to its poor mechanical strengths as a bulk.

In scaffold production, polymers are considered as basic materials widely used in tissue engineering applications [10]. A polymer is a natural or synthetic macromolecule composed of small repeated units called monomers. To be used in advanced prosthetic applications, a polymer scaffold is required to show high biocompatibility, proper biodegradability, high porosity with proper pore size, and proper pore distribution with high specific area. For adequate nutrients to be transported for cell ingrowth, a desirable scaffold needs to have proper pore size and shape [11]. To be able to tailor scaffold pore size and shape is a critical factor for scaffold morphology optimization.

The formation of polymer fibers processed by electrospinning has been explored by some groups of researchers since its patented introduction by Formhals in 1934 [12-14]. Electrospinning is a fiber production technology that can generate polymer nanofibrous mats that contain fibers ranging from 50 to 500 nm in diameter consistently [15]. The advantages of non-woven polymer nanofibers are that it enables a control of pore size and have a great potential to be scaffolds for cell growth.

Thus, fabrication of scaffolds by combining bioactive ceramics such as hydroxyapatite and polymers to develop ceramic-synthetic polymer composites by electrospinning carries a great potential to create the most desirable biodegradable scaffold with sufficient mechanical strength and highly porous structure by mimicking the architecture of natural bone.

CHAPTER 2

BACKGROUND

2.1 Bone Biology

Bone is consists of two types of tissues: compact (accounts for about 80% of the total skeleton) and spongy (cancellous) (accounts for about 20% of total skeleton). The major difference in these two tissues is how dense and tightly the tissues are packed. In bone homeostasis, three types of cells in bone contribute: osteoblast, osteoclast, and osteocyte (Table 2.1). Osteoblast accounts for bone formation, osteoclast works to break down and resorb bone, and osteocyte are bone cells that are matured.

Table 2.1 Bone Cell Types and Their Morphologies and Functions

Cell type	Morphology	Function
Osteoblast	Cuboidal shape Polarized and located at the bone surface	Synthesis and regulation of bone ECM deposition and mineralization Respond to mechanical stimuli
Osteocytes	Satellate shape Possesses fewer organelles than osteoblasts	Calcification of osteoid matrix Blood calcium homeostasis Mechanosensor of the bone
Osteoclasts	Polarized cells, Multinucleated	Bone resorption

Compact bone is composed of packed osteon and haversian. Haversian is a central canal that is located in osteon and it is surrounded by concentric rings of matrix. Osteocyte , the matured bone cell, is located in a space called lacunae between the rings of matrix. Canaliculi spread from lacunae to harversian canal providing passages through hard matrix. Osteonic canals include blood vessels.

Spongy (cancellous) bone is less dense and lighter compared to the compact bone. Spongy bone is composed of trabeculae and bars of bone that are adjacent to small cavities which contain red bone marrow (Figure 2.1). To receive a blood supply, canaliculi are connected to the adjacent cavities. The trabeculae is arranged to provide maximum strength. Trabeculae located in spongy bone follows the lines of stress and when the direction of stress applied changes, it can also realign.

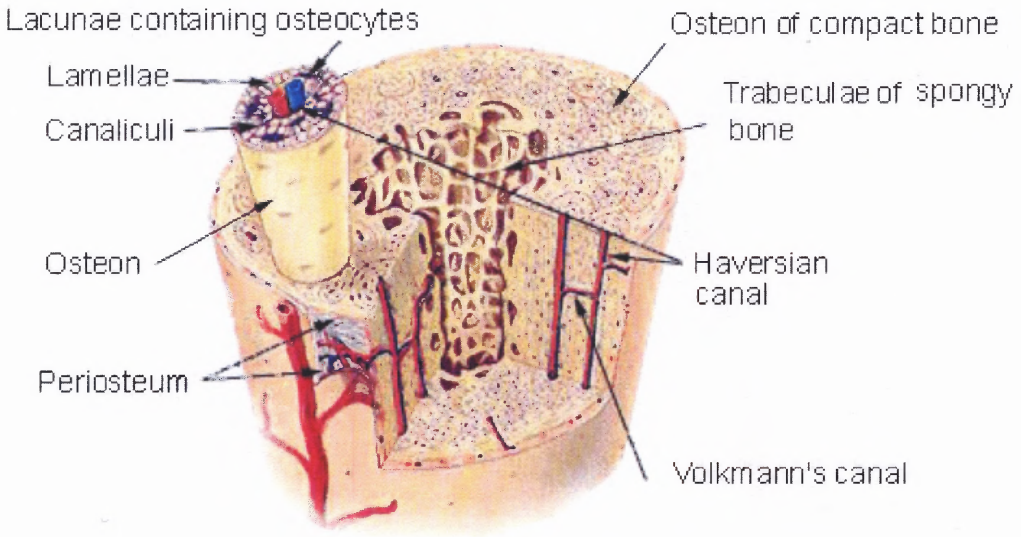

Figure 2.1 Structure of bone, compact bone and spongy (cancellous bone) [1].

2.2 Bone Tissue Engineering

The term "tissue engineering" was defined in 1988 as "The application of the principles and methods of engineering and the life sciences toward the fundamental understanding of structure-function relationships in normal and pathological mammalian tissue and the development of biological substitutes that restore, maintain, or improve tissue function" [17]. Whereas the classic biomaterial approach is based on the implantation of spare

parts, tissue engineering is based on the tissue formation and regeneration that leads to the formation of new functional tissues. For the successful tissue engineering application, the understanding and integration of physics, biology, chemistry, material science, engineering, and medicine is essential.

In bone tissue engineering, bone cells, extracellular matrix, intercellular communications, growth factors, and cell-matrix interactions are some components to be understood from a biological perspective [18]. In addition to this, another important factor in bone tissue engineering is the three dimensional structure of the bone. Since cells do not grow in a three dimensional manner in vitro, designing a scaffold that mimic the bone structure is crucial for the cells to grow to form a new tissue in three dimensional manner in vivo [18].

2.2.1 Scaffolds for Bone Tissue Engineering

A scaffold is a temporary template for cells to regenerate and restore functional tissues. Scaffolds for bone provide cells with a tissue specific environment and architecture in three dimensional. Scaffolds support and provide a reservoir for nutrients, water, cytokines, and growth factors.

In vivo, cells use scaffolds as a temporary matrix where they can deposit and proliferate to induce bone ingrowth, until new bone tissue is fully restored. Scaffolds also act as a template for a vascularization of newly formed tissues [19]. Engineering a scaffold requires the development of a series of properties that will be discussed later.

2.2.2 Essential Properties for a Desirable Scaffold

Researchers have been devoted to bone tissue engineering where they develop desirable three dimensional porous scaffolds with tissue-inducing factors [5, 18, 19]. The three dimensional porous scaffolds need to be designed so that they play an important role manipulating osteoblasts functions as well as guide and induce new bone formation. Materials used in scaffolds also need to be osteoconductive for osteoprogenitor cells to migrate and adhere onto the scaffolds, differentiate and form a new bone [6, 7]. The desirable scaffolds should be also biodegradable with proper degradation rate so that the scaffolds will eventually be replaced totally by newly formed bone.

Porosity is also important. Scaffolds should have fully interconnected highly porous structure with high surface to volume ratio for cell ingrowth and vascularization for newly formed tissue [19]. Thus the scaffold in bone tissue engineering should satisfy the requirements: biocompatiblility, osteoconductivity, osteoinductivity, interconnected porous structure, proper biodegradability, and proper mechanical strength.

2.2.3 Osteoconduction

Osteoconduction is a process where bone cells from recipient host bed migrate into the three dimensional bone implant and new bone is formed as a result of the cell migration. In successful bone engineering, osteoconductivity is crucial for an implant to integrate into the host site. Bone tissue, minerals and collagenous components are osteoconductive. Osteoconduction is observed in highly porous implant similar to bone structure.

Osteoconductive materials serves as a scaffold on which bone cells can attach, migrate, and grow. Osteogenic cells work better when they have a scaffold to attach to. Porous biodegradable polymers, bioactive ceramics including hydroxyapatite, and collagen hydroxyapatite combinations are all osteoconductive [20]. When the materials used for the implant have low biocompatibility, the implant does not show much osteoconductivity.

2.2.4 Osteoinduction

Osteoinduction is a process where osteoprogenitor cells, immature bone cells, are recruited to a bone healing site and an osteogenic differentiation pathway is induced to produce preosteoblasts [21]. This induction of osteogenic differentiation pathway is called osteogenesis.

Osteoinduction is seen in all type of bone healing process. The majority of bone healing depends on this osteoinduction process. Osteoinductive materials induce new bone formation by stimulating osteogenic cells.

In case a portion of bone to be regenerated is large, natural osteoinduction with the presence of a scaffold may not be enough for a total tissue regeneration [18]. For this reason, a scaffold with its own osteoinductivity is essential for a successful integration of the scaffold to the host site.

2.3 Biomaterials Used in Bone Tissue Engineering

The selection of materials used to produce scaffolds for bone tissue engineering application is very important since the properties of scaffolds rely on the properties of the materials used to a great extent. The materials proposed for the scaffold production so far are metals, ceramics, and polymers [18].

To achieve a successful osteointegration of a scaffold, bioactive ceramics such as hydroxyapatite, tricalcium phosphate and biodegradable polymers have been selected by a number of researchers. Current study indicates that ceramics shows exceptional biocompatibility properties, interacting bone cells and tissues and carries a great potential for bone tissue engineering application [8, 9]. The biodegradable polymer is biodegradable and its biodegradability is controllable.

2.3.1 Hydroxyapatite

Chemical Formula of Hydroxyapatite: $Ca_{10}(PO_4)_6(OH)_2$

Hydroxyapatite was first identified as one of the mineral components of mammalian hard tissue and bone in 1926 [22]. About 25 years ago, synthetic hydroxyapatite was started to be considered as a potentially useful biomaterial in dentistry, orthopedics and bone grafts [23]. Through the intensive studies of hydroxyapatite based scaffolds, hydroxyapatite is known to show good bone bonding ability and osteocoductivity in vivo [18]. Due to its ability to support osteointegration and bone ingrowth in its tissue engineering applications, hydroxyapatite is classified as one of the few biomaterials known as bioactive materials [19].

Hydroxyapatite has been known to be osteoconductive through a number of researches conducted in the past. Nagashima et al. conducted an experiment to investigate the osteoconductivity of a porous hydroxyapatite block [24]. The porous hydroxyapatite blocks were designed to have mean pore diameter of 90 microns and with 70% porous volume. The blocks were implanted into the dog's defect site of lamina. The blocks were taken out and examined after 3 months and 6 months.

The result showed new bone formation in the pores of the blocks and bone growth occurred more frequently in the part close to the original bone than in the other parts of the porous hydroxyapatite blocks implanted. Similar research had been conducted by Boyde et al. and Yuan et al. and both cases of porous hydroxyaptite implants achieved osteoconduction [25, 26]

Hydroxyapatite, however, is also known to have poor mechanical strengths as a bulk material. For this reason, dense hydroxyapatite cannot be used for long term load bearing applications in spite of its beneficial biocompatible properties [23]. To overcome its physical inadequacies with bulk, hydroxyapatite is often used as a coating for metallic implants such as titanium/titanium alloys and stainless steels. This way, the resulting implants enable the bone cells to interact with hydroxyapatite to react with, while bioinert metallic parts provide the mechanical strength required without being considered as a foreign body or being isolated from the surrounding tissues. Hydroxyapatite is also non-degradable and it has been shown to remain intact over a period of ten years in the body [51].

Hydroxyapatite in forms of porous blocks and powders can also be used as bone fillers. The hydroxyapatite filler provides scaffolds for naturally forming bones reducing a healing time and it also become a part of the bone structure [27].

2.3.2 Advantages and Disadvantages of Hydroxyapatite Incorporated Implants

Hydroxyapatite is often used as a coating of metallic implants such as titanium/titanium alloys and stainless steels. This way, the resulting implants enable the body to see hydroxyapatite to react with, while bioinert metallic parts providing the mechanical strength required without being considered as a foreign body or being isolated from the surrounding tissues.

The optimization of coating quality and the effects of coating resorption, however, are yet to be discussed. If the resorption of the coating is not kept at the optimal levels, disintegration of the coating resulted by the resorption can reduce the bonding strength formed between the bone and the implant and this may result in the complete loss of the implant [28].

The hydroxyapatite coating have been done by a variety of methods include dip coating into a powder suspension, electrophoretic deposition, electron beam evaporation combined with ion beam mixing, laser ablation, sol-gel, plasma spray, rf sputtering methods [28]. These coating methods, however, have advantages and disadvantages. The summary of advantages and disadvantages of each coating method is described in Table 2.2.

Table 2.2 Summary of Hydroxyapatite Coating Methods [49]

Method	**Thickness of the coating**	**Advantages**	**Disadvantages**
Dip Coating	0.05-0.5mm	Inexpensive Coatings applied quickly Can coat complex substrates	Requires high sintering temperatures Thermal expansion mismatch
Sputter Coating	0.02-1μm	Uniform coating thickness on flat substrates	Line of sight technique Expensive, Time consuming Cannot coat complex substrates Produces amorphous coatings
Pulsed Laser Deposition	0.05- 5μm	As for sputter coating	As for sputter coating
Hot Pressing and Hot Isostatic Pressing	0.2-2.0mm	Produces dense coatings	HP cannot coat complex substrates High temperature required Thermal expansion mismatch Elastic property differences Expensive, Removal/Interaction of encapsulation material
Electrophoretic Deposition	0.1-2.0mm	Uniform coating thickness Rapid deposition rates Can coat complex substrates	Difficult to produce crack-free coatings Requires high sintering temperatures
Thermal Spraying	30-200μm	High deposition rates	Line of sight technique High temperatures induce decomposition, Rapid cooling produces amorphous coatings
Sol-Gel	<1μm	Can coat complex shapes Low processing temperatures Relatively cheap as coatings are very thin	Some processes require controlled atmosphere processing Expensive raw materials

2.3.3 Biodegradable Polyester

A polymer is a natural or synthetic macromolecule composed of smaller repeated units called monomers. Many synthetic polymers are resistant to physical and chemical degradation and thus disposal related issues are raised after use of the synthetic polymers. For this reason, biodegradable polyesters such as poly(glycolic acid) (PLG), poly(lactic acid) (PLA), and their copolymer poly(lactide-*co*-glycolide) (PLGA) have been extensively studied for their potentials in biomedical and pharmaceutical applications over the past few decades [29, 30].

The biodegradable polyester is one of the few synthetic polymers that are biodegradable and its biodegradability is controllable. Through degradation, PGA, PLA, and PLGA transform into non-toxic substances and will be removed from human body. In tissue engineering, biodegradable polyesters are often used to create a biodegradable scaffolds which have controlled degradation rate [29].

2.3.4 poly(L-lactic acid) (PLLA)

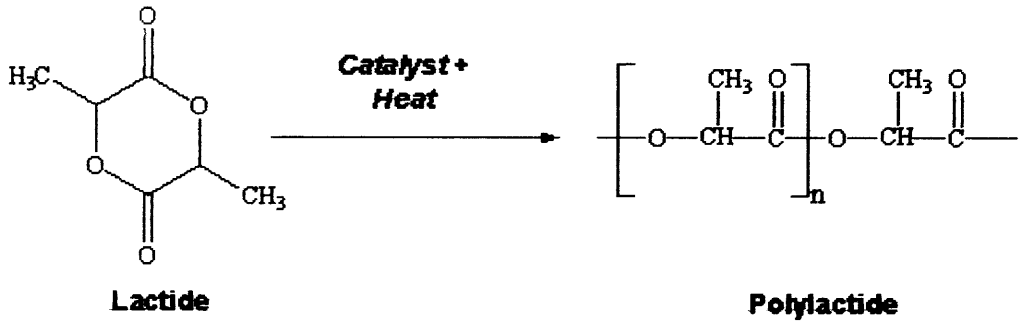

Figure 2.2 Ring-opening polymerization of lactide to obtain polylactide [31].

Polylactic acid or Polylactide is a biodegradable aliphatic polyester derived from lactic acid. Polylactic acid/Polylactide is produced through ring-opening polymerization using catalyst (Figure 2.2). Poly(L-lactic acid) (PLLA) is a resulting product of lactic acid polymerization in the L form.

The crystallinity of PLLA is around 37%, its glass transition temperature is between 50 ° C ~ 80 ° C, and its melting temperature is 173 ° C~178 ° C. Like most thermoplastics, polylactic acid can be processed to form fibers and films. Due to its biodegradable properties, polylactic acid is used widely in various biomedical applications and evaluated for tissue engineering. The price of PLA is higher than many petroleum derived plastics; however, it has been falling as production of PLA increases.

2.3.5 poly(lactide-*co*-glycolide) (PLGA)

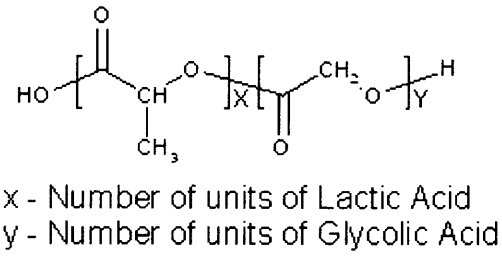

Figure 2.3 Structure of poly(lactic-*co*-glycolic acid) [32].

Poly(lactide-*co*-glycolide) (PLGA) is a FDA approved copolymer of PLA and PGA. PLGA is synthesized by random ring-opening copolymerization of lactic acid and glycolic acid (Figure 2.4). Successive monomer units of lactic acid and glycolic acid are linked together by ester linkages during polymerization of PLGA and yield a linear aliphatic polyester as a final product (Figure 2.3).

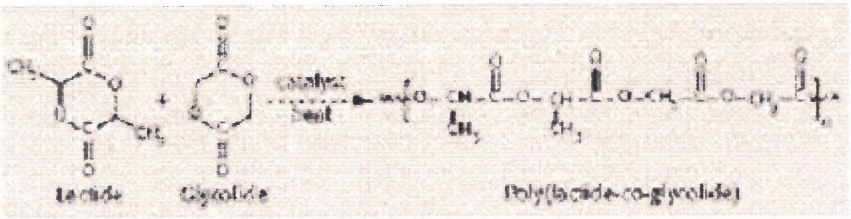

Figure 2.4 Synthesis of poly(lactic-*co*-glycolic acid) [33].

The ratio of lactide to glycolide monomers used in the polymerization determines the content of the comonomers in the final polymer, such as PLGA 75:25 which identifies a copolymer of 75% lactic acid and 25% glycolic acid composition. PLGA has a glass transition temperature in the range of 40 – 60°C and is amorphous rather than crystalline (Figure 2.5).

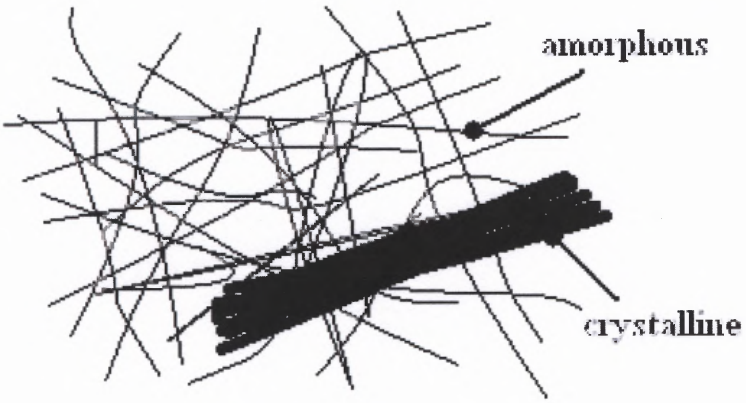

Figure 2.5 Polymer network structure: crystalline (bundles) phase and amorphous (dispersed) phase of polymer.

Different from homopolymers of lactic acid and glicolic acid which have poor solubilities, PLGA can be dissolved in wide range of solvents such as chlorinated solvents, tetrahydrofuran, ethyl acetate, and acetone.

In the presence of water, hydrolysis of its ester linkage leads degradation of PLGA into non-toxic substances and will be removed from human body. The degradation time of PLGA is related to the ratio of monomers used in polymerization; the higher the number of glycolides, the lower the PLGA degradation time required. There is an exception, however, that PLGA 50:50 exhibits faster degradation time. In the body, PLGA produces lactic acid and glycolic acid through hydrolysis. These two substances are by-products of metabolic pathways in the body under a normal physiological condition. The alteration of the monomer ratio of PLGA during its synthesis enables to control the degradation time of PLGA. Due to its high biodegradability and biocompatibility, PLGA is currently used widely in biomedical and pharmaceutical applications.

2.4 Electrospinnig

Electrospinning is a polymer processing method in which polymer solution is transformed into a fine fiber and deposited onto a collector plate by electrostatic force. This method is patented by Formhals in 1934, and since then the formation of polymer fibers processed by electrospinning has been explored by several researchers [12-14]. Electrospinning can generate polymer nanofibrous mats that contain fibers ranging from 50 to 500 nm in diameter consistently [15]. The advantages of non-woven polymer nanofibers are that it enables a control of fiber diameter and have a great potential to be scaffolds for cell growth.

2.4.1 The Setup and a Principle of Electrospinning

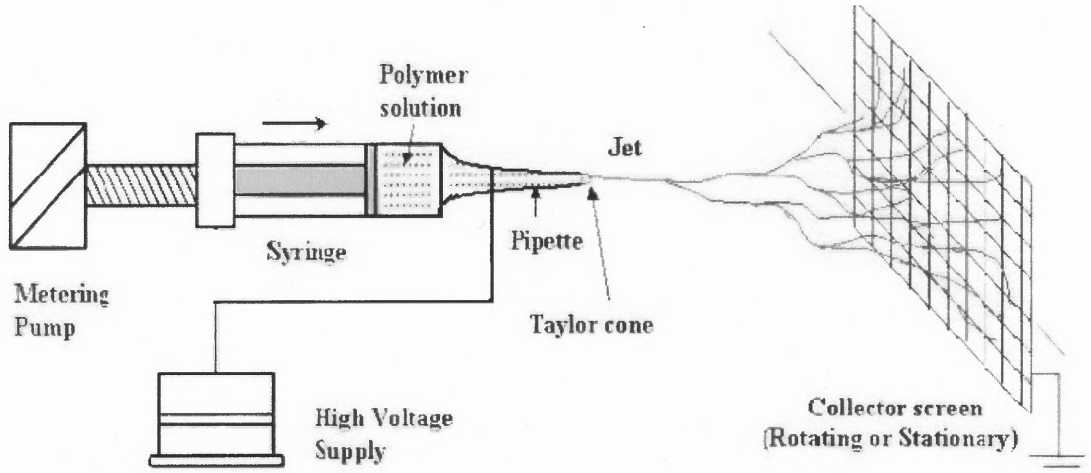

Figure 2.6 Apparatus of electrospinning [34].

Electrospinning system consists of two major parts: a collector and a sprayer (Figure 2.6). The sprayer consists of syringe with needle which contains a polymer solution to be electrospun and syringe pump which pushes the polymer solution at a certain rate. The collector plate collects the fibers that are drawn from the tip of the syringe needle. The collector screen and the syringe needle are attached to the high voltage DC power supply. The syringe needle is attached to the positive output of the high voltage power supply. In electrospinning system, the applied voltage ranges from 7 kV to 30 kV. This range of the voltage being applied is high enough so that the surface tension of a polymer solution can be overcome to form a fiber. The electrostatic force between the tip of the needle and the collector screen induce the formation of fiber jets from the tip of the needle and the positively charged fibers travel to the surface of the collector screen.

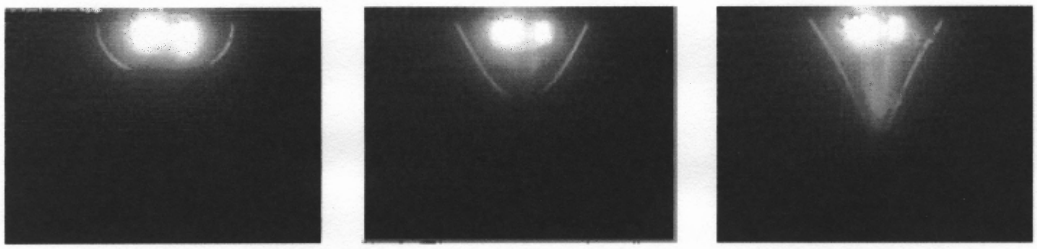

(a) stage 1 (b) stage 2 (c) stage 3

Figure 2.7 Formation of the Taylor cone. Voltage increases with each stage until equilibrium between the electrostatic force and surface tension is achieved in stage 3 [35].

When the electrostatic force and the surface tension of the polymer solution is at equilibrium, the solution forms a cone shape at the tip of the needle in the electrospinning process (Figure 2.7). This cone is called Taylor cone and was described first by Sir Geoffrey Ingram Taylor in 1964 [36]. Taylor cone is observed only in viscoelastic, Newtonian, and inviscid liquids [37].

Taylor's primary interest was the behavior of water droplets in a strong electric field. According to Taylor's theory, a semi-vertical angle of 49.3^{o} is required to form a perfect cone under the described condition. Taylor demonstrated a formation of theoretically described cone shape before jet formation and the semi-vertical angle is known as Taylor angle [36].

When the electrostatic force between the collector plate and the tip of the needle overcome the surface tension of the polymer solution coming out from the tip of the needle, fibers start to be drawn from the tip of the Taylor cone. As the fibers travel to the collector plate, the solvent contained in the polymer solution evaporates leaving non-woven polymer fabrics. This fiber formation is observed only when the polymer

concentration in the solution to be electrospun is high enough to cause molecular chain entanglement. Otherwise, droplets are dispersed to the collector.

Using electrospinning method, a wide range of polymers can be processed to form nanofibrous mats. Those polymers include cellulose derivatives, polylactides, polyamides, polyethyleneoxide, and polymers contain solid nanoparticles or small molecules.

2.4.2 Advantage of Scaffold Processing by Electrospinning

The great advantage of electrospinning method its ability to create unusually small fiber mats which range from micro- to nano- size (Figure 2.8). The nanofibrous mats fabricated by electrospinning have high surface area to volume ratio and a fiber size can also be controlled. By creating the high surface area to volume ratio, electrospinning enables the fabrication of three-dimensional scaffolds that mimic the architecture of extracellular matrix (ECM) including bone [38].

The nanofibrous scaffold carries the potential for a number of applications. Those possible applications range from wound dressing materials, artificial organs, protective clothing, separation membranes, sensors and nano-composites.

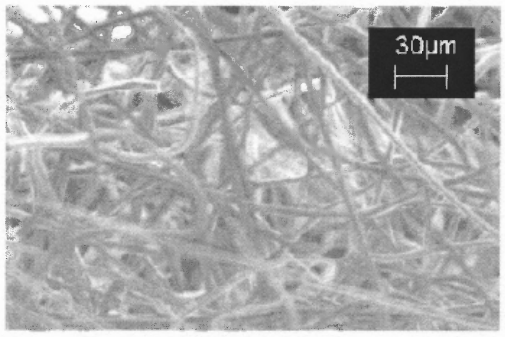

Figure 2.8 Electrospun PLLA nanofibrous mats.

2.5 Biomimetic Process with Simulated Body Fluid (SBF)

The development of three-dimensional nanofibrous scaffold with hydroxyapatite coating can be also achieved by biomimetic process using simulated body fluid (SBF) developed by Kokubo [39]. Biomimetic refers to a laboratory procedure designed to imitate a natural chemical process. Recent research shows the biomimetic process is one of the most promising tissue engineering techniques that can produce bioactive apatite coating at ordinary temperature and pressure [40]. Kokubo et al. developed an acellular SBF with inorganic ion concentrations similar to natural human blood plasma (Table 2.3).

Table 2.3 Ion Concentration of The Simulated Body Fluid and Human Blood Plasma [41]

Ion	Concentration (mol/m^3)	
	Simulated Body Fluid (SBF)	Human Blood Plasma
Na^+	142.0	142.0
K^+	5.0	5.0
Mg^{2+}	1.5	1.5
Ca^{2+}	2.5	2.5
Cl^-	147.8	103.0
HCO_3^-	4.2	27.0
HPO^{3-}	1.0	1.0
SO^{2-}	0.5	0.5

SBF is prepared to have calcium and phosphate ions supersaturated with respect to apatite. When a substrate is immersed in the SBF, the heterogeneous nucleation of calcium phosphate induces the formation of apatite layer on the substrate in vitro at pH=7.4 and temperature 37 °C (Figure 2.9).

Heterogeneous nucleation is the process of initiation of a new phase in a supersaturated solution environment and the nucleation system contains two or more components. SBF is a metastable solution. The solution is in a state of pseudo-equilibrium that will change if disturbed in some manner.

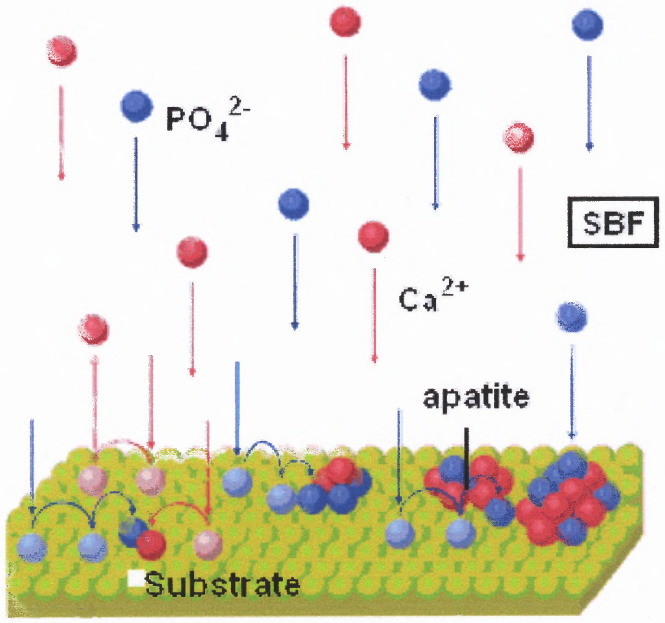

Figure 2.9 Heterogeneous nucleation containing multiple components [42]. Nucleation of calcium and phosphate ions induces the formation of apatite layer on the surface of the substrate.

To promote a formation of apatite through heterogeneous nucleation, a 1.5 SBF solution with 1.5 times each ion concentration of SBF is proposed by Kokubo et al [43] (Table 2.4). The preparation procedure of Kokubo's SBF and 1.5 SBF are stated in appendix A.

Table 2.4 Modification of Ion Concentration in SBF [41]

Ion	Concentration (mol/m^3)	
	SBF	1.5 SBF
Na^+	142.0	213.0
K^+	5.0	7.5
Mg^{2+}	1.5	2.3
Ca^{2+}	2.5	3.8
Cl^-	147.8	221.7
HCO_3^-	4.2	6.3
HPO^{3-}	1.0	1.5
SO^{2-}	0.5	0.8
pH	7.25	7.25

The formation of apatite incorporated nanofibrous polymer scaffold can be achieved by the combination of an electrospun mat with SBF solution. This combination defines a biomimetic method. For this study bioceramics/polymer composite scaffolds are developed by electrospinning.

2.6 Literature Review

A number of fabrication methods of ceramics/bioglass coated three dimensional scaffold has been suggested to this date, and its properties, structure, biocompatibility, osteoconductivity, and the effect of ceramics/bioglass content have been intensively studied by several researchers.

Lu et al. conducted an experiment to determine the effects of bioglass (BG) content on the maturation of osteoblast-like cells on the PLGA-BG composite developed by solvent-casting followed by biomimetic process [44]. Lu developed PLGA-BG composite with its BG content of 0 wt%, 10 wt%, and 50 wt% and monitored the cell

proliferation, alkaline phosphatase activity and mineralization as a function of BG content and culturing time.

In her study, Lu found that the kinetics of calcium phosphate layer formation, and the response of human osteoblast-like cells were dependent on BG content of the PLGA-BG composite; the 10 wt% and 25 wt% BG composite supported greater osteoblast growth and differentiation compared to the 50 wt% BG group. The study by Lu suggests that there is a threshold BG content that is optimal for osteoblast growth, and the interaction between PLGA and BG may modulate the kinetics of calcium-phosphorus formation and the overall cellular response [45].

Causa et al. conducted a study to analyze the mechanical properties, structure, biocompatibility, and osteoconductivity of polymer-HA composite [46]. The HA particles were added to the polycaprolactone (PCL) matrix and three PCL-HA composites with HA content of 13 wt%, 20 wt%, and 32 wt% were developed. In their study, it was found that composite of 20% and 32% HA led to a significant improvement in mechanical performance of scaffold. The PCL-HA composite was also found to improve osteoconduction compared to the PCL alone [43].

Laurencin et al. conducted a study to examine the in vitro attachment and growth of bone morphogenetic protein (BMP)-producing cells on a PLAGA-HA scaffold [44]. In their study, Laurencin et al. found that the polymer-ceramic scaffold supported bone morphogenetic protein-2 (BMP-2) production, allowing the attachment and growth of retroviral transfected, BMP-2-producing cells. It was also found that in vivo, the scaffold functioned as a delivery vehicle for bioactive BMP-2, as it induced heterotopic bone formation in a SCID mouse model [44].

CHAPTER 3

RESEARCH OBJECTIVE

The purpose of this study is to determine the potential of fabricating hydroxyapatite (HA) and polymers (PLLA and PLGA) by electrospinning to form synthetic composite materials for bone tissue engineering applications. The nanofibrous mats obtained by electrospinning follow characterization using scanning electron microscope (SEM) - Energy Dispersive X-ray Analysis (EDXA), Thermogravimetric Analysis (TGA), and X-ray Diffraction (XRD) and the morphology, chemical composition, wt% of HA deposit, and the identification of mineral components of the electrospun mats are analyzed.

CHAPTER 4

EXPERIMENTAL METHODS

4.1 Electrospinning Equipment

In this experiment, the electrospinning apparatus was set as in Figure 4.1. The apparatus consists of syringe pump, syringe with polymer solution loaded inside, needle attached to the syringe, collector screen, and high voltage power supply.

The collector screen and the syringe needle are attached to the high voltage DC power supply. The syringe needle is attached to the positive output of the high voltage power supply [Gamma High Voltage Power Supply ES30P, Gamma High Voltage Research, Ormond Beach, FL].

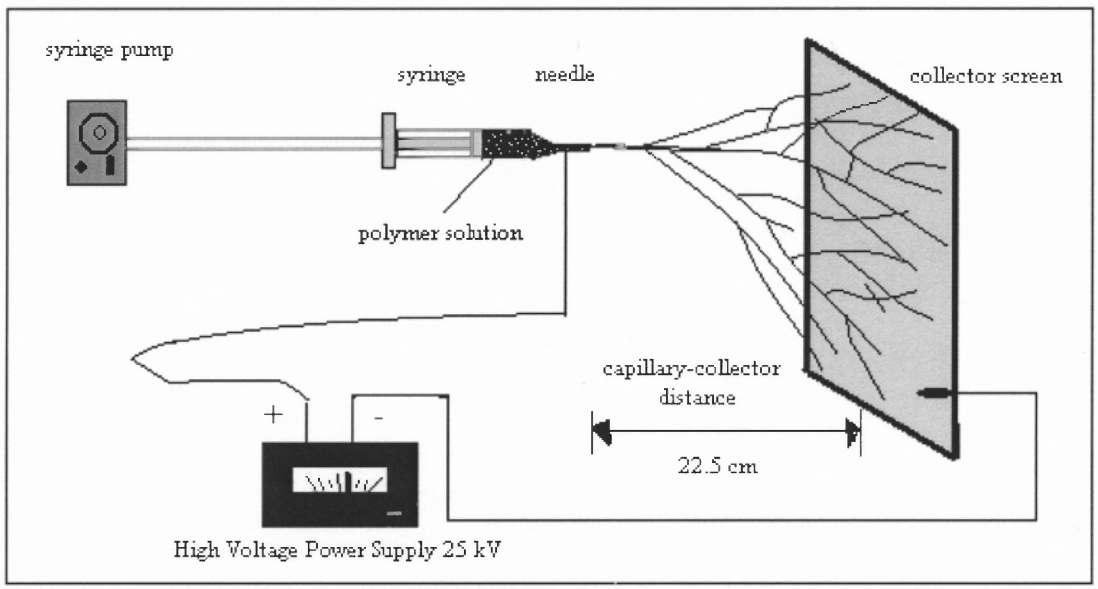

Figure 4.1 Electrospinning setup.

The syringe with polymer solution loaded inside is mounted on a syringe pump [Harvard Syringe Pump Model 901]. In this experiment, the electrospinning process was performed with a constant syringe pump flow rate of 0.103 ml/min, 25 kV power supply voltage, capillary – collector distance 22.5 cm, and size 12-gauge and 20-gauge needles. The size 12-gauge needle was used to create micro size electrospun fibers and the size 20-gauge needle was used to create nano size electrospun fibers. Copper metal was used as a collector for this experiment.

4.2 Materials

Two types of polymers were used in this electrospinning experiment: poly(L-lactic acid), Resomer® L207 [Boehringer Inglheim Fine Chemicals] and poly(lactide-*co*-glycolide), 7525DL High IV [Alkermes, INC]. Both PLLA and PLGA are FDA approved biodegradable polyesters which transform into non-toxic substances in vivo.

The solvent used to create 10%wt polymer solution of PLLA and PLGA was methylene chloride [Fisher Scientific]. Ceramics used in this experiment was hydroxyapatite powder [product #289396, Sigma-Aldrich]. Hydroxyapatite is known to have good bone bonding ability and osteocoductivity in vivo.

4.3 Solution Preparation

4.3.1 Electrospinning of HA/Polymer solution

The solutions of poly(L-lactic acid) (PLLA) and methylene chloride of 10 wt% and poly(lactide-*co*-glycolide) (PLGA) and methylene chloride of 10 wt% were prepared. To create solutions of 10 wt% concentrations, 5 grams of PLLA and 5 grams of PLGA were

dissolved in 45 grams of methylene chloride each and mixed thoroughly. Hydroxyapatite (HA) powder were ground using mortar and pestle to achieve the powder size of 3 ~ 10 μ m. The ground HA powder was measured and added to the three PLLA solutions and three PLGA solutions prepared previously so that the HA powder added in each solution to account for 0, 10, and 25 wt% of the total solids. The following two different methods were used for the addition of HA powder into polymer solutions, to compare the dispersion of HA powder in resulting electrospun mats.

Method 1:

The HA powder measured was added to each polymer solution. The solutions were then mixed overnight with magnetic stirrer. This was followed by the electrospinning process.

Method 2:

The addition of HA powder to each polymer solution was carried out within five minutes before the electrospinning of solution to prevent the formation of large HA lumps in the nanofibrous mats. The HA-polymer solutions were mixed well right before the electrospinning process.

The HA-polymer solutions with 0 HA wt% were used as a control. Each solution was electrospun separately using 12-gauge and 20-gauge needles (Table 4.1). The parameters for this electrospinning process were kept constant: voltage 25kV, flow rates 0.103 ml/min and the distance form the collector 22.5cm.

Table 4.1 Solutions Prepared to be Electrospun

Polymer solution	PLLA						PLGA					
HA wt%	0%		10%		25%		0%		10%		25%	
Gauge size LF- 12-gauge SF- 20-gauge	LF	SF	LF	SF	LF	SF	LF	SF	LF	SF	LF	SF

4.3.2 A Biomimetic Protocol for Electrospun Mats with SBF

Following is the biomimetic experiment using SBF to create apatite coated polymer nanofibrous scaffolds. In this process, the electrospun nanofibrous polymer mats are immersed in SBF solution.

Solution of PLLA and methylene chloride of 10 wt% and solution of PLGA and methylene chloride of 10 wt% were prepared. Both solutions were electrospun using two different needle sizes: 12-gauge needle (LF), and 20-gauge needle (SF). The parameters for this electrospinning process were kept constant: voltage 25kV, flow rates 0.103 ml/min and the distance to the collector 22.5cm. Total of 32 samples were punched out in the size of 5mm diameter flower shape from the electrospun nanofibrous mats; eight samples from PLLA LF mats, eight samples from PLLA SF mats, eight samples from PLGA LF mats, and eight samples from PLGA SF mats.

The samples were immersed in an aqueous suspension of 0.2 wt% calcium hydroxide at 40 ℃ for 24 hours being shaken at a rate of 60 times/min. After being treated with calcium hydroxide, two samples from each mat were used as a control group and were not treated with SBF. Three samples from each control were then immersed in a regular concentration of SBF and the other three samples were immersed in a 1.5 SBF and kept for one week at pH 7.25 at 36.5 ℃.

4.4 Characterization of HA/Polymer Electrospun Mats

The electrospun mats obtained followed characterization using Scanning Electron Microscope (SEM) - Energy Dispersive X-ray Analysis (EDXA), Thermogravimetric Analysis (TGA), and X-ray Diffraction (XRD) and the morphology, chemical

composition, wt% of HA deposit, and the identification of mineral components of the electrospun mats were analyzed respectively.

In SEM-EDXA, pure HA powder was analyzed as a reference. The pure PLLA and PLGA electrospun mats with 0% HA were used as controls for TGA to obtain accurate wt% of HA particles in 10% and 25% HA incorporated electrospun mats. In XRD, both pure HA powder and pure PLLA and PLGA electrospun mats were used as references for identification of the corresponding peaks observed in 10% and 25% HA incorporated mats.

4.4.1 Scanning Electron Microscope (SEM)

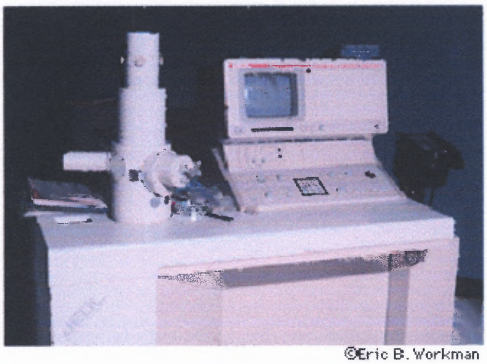

Figure 4.2 Scanning electron microscope [47].

The formation, fiber and HA distributions, and morphology of the nanofibrous mats were observed using scanning electron microscope (SEM) in this study (Figure 4.2).

The SEM is designed for a direct study of the surface of solid objects. Unlike traditional optical microscopes that use lenses to bend the light waves, SEM uses

electromagnets to bend an electron beam to form images. By using electrons, SEM enables observers to have a better control in desired magnification management and also provides better clarity in images. Since SEM has a large depth of the field, large area of sample can be focused at one time. It can also produce high resolution images allowing closely spaced features to be examined at high magnification. For this reason, the image that has good representation of the sample's three-dimensional structure is produced by SEM.

In this study, two SEM images were taken for each sample. The mean fiber diameter of the resulting electrospun mats were quantified by analyzing the measurements of ten randomly selected fibers per SEM image.

Sample Preparation:

The only requirement for the SEM sample is to be electrically conductive and thus the preparation of the samples is not difficult. Since metals are electrically conductive, no preparation is required to be viewed by SEM. To examine non-conductive metals such as ceramics and plastics, however, the samples need to be coated with a thin layer of a conductive material such as gold or carbon.

Carbon Coating:

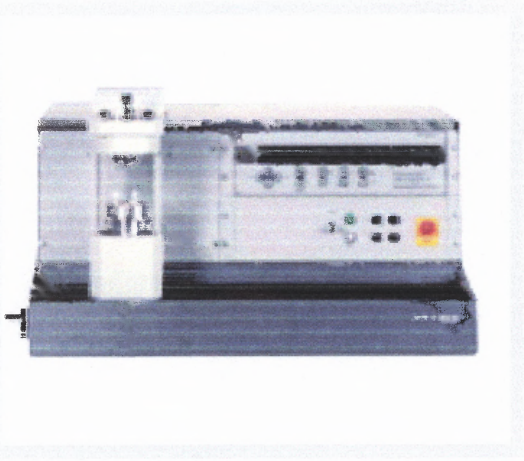

Figure 4.3 Carbon coater [48].

To examine non-conductive samples, carbon coating method is often used to provide a conductive layer on the samples by carbon coater (Figure 4.3). Carbon films are used due to their mechanical stability, low background signal, and good electrical conductivity. The films of their thickness 50 nm or more are used in SEM preparation.

To achieve the coating, a high vacuum evaporator with carbon fiber is commonly used. In a carbon coater, a carbon fiber burns and evaporates within a second or less at high temperature leaving a carbon coating on a sample. This quick evaporation process is called a "flash evaporation". The evaporation depends on the surface area, length of the fiber, and the temperature.

Mechanisms of SEM:

In SEM, electron beam is produced at the top of the microscope by heating metallic filaments. The electron beam passes vertically through the microscope column. When the beam reaches to the electromagnetic lenses, the beam is directed down towards a sample. Once the beam hits the sample, secondary (or backscattered) electrons are produced from

the sample. The secondary electrons are collected by detectors and converted to a signal that produces an image on the screen (Figure 4.4).

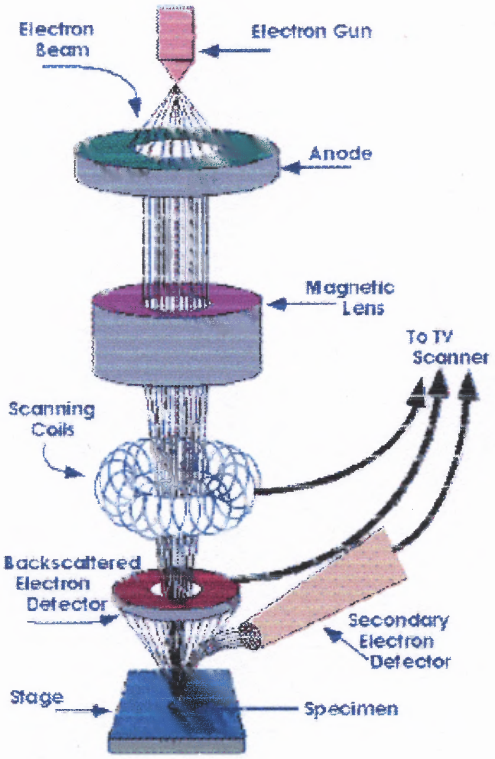

Figure 4.4 Electron path of SEM [50].

Vacuum:

When a SEM is used, the column and sample must always be at vacuum. A vacuum environment means that most of the air molecules have been removed from the inside of the microscope. There are many reasons for requiring a vacuum in an SEM. If the filament were surrounded by air, it would quickly burn out, like a light bulb. If the column were full of air, the electrons would collide with the gas molecules and never reach the sample. If gas molecules react with the sample different compounds could form and condense on the sample. This can lower the quality of the image.

4.4.2 Energy Dispersive X-ray Analysis (EDXA)

The elemental compositions of samples are analyzed using Energy Dispersive X-ray Analysis (EDXA) following a pre-coating of samples with carbon. EDXA is a qualitative analysis that involves the identification of the elements present in the area of a sample irradiated by electron beam. This process is accomplished by identifying the fluorescent characteristic x-rays emitted from the irradiated area of the sample.

EDXA is accomplished by extremely rapid process. The entire x-ray spectrum of the sample can be acquired in a matter of seconds. EDXA allow users to estimate the chemical stoichiometry of the sample since the relative intensity of x-ray in the spectrum is proportional to the abundance of elements in the sample. EDXA also involves semi-quantitative approach that can provide an estimate of elemental weight fractions, or atomic proportions of the sample. Since the detection of x-ray does not depend on beam-sample-detector geometry, EDXA is an effective method to characterize rough samples such as loose grains or unpolished materials. The weak intensities of x-ray produced by the elements at trace levels limit the qualitative approach of EDXA.

In this study, the weight % ratio of P/Ca in EDXA result at 500X was compared to the elemental weight % ratio of P/CA=2.16 of HA for the confirmation of the presence of HA in the sample.

4.4.3 Thermogravimetric Analysis (TGA)

A quantitative measurement of mass change of nanofibrous mats associated with thermal degradation was obtained using Thermogravimetric Analysis (TGA). The mass change of materials from dehydration, decomposition, and oxidation of samples with time and temperature was observed for a quantitative purpose.

TGA is widely used for the testing of materials such as polymers, composites, adhesives, food, chemicals, and organic materials. TGA uses heat to force physical changes and reactions in the sample. The quantitative measurement of mass change in the sample is associated with transition and thermal degradation. The change in mass from dehydration, decomposition, and oxidation with time and temperature is recorded in TGA. The thermogravimetric curves are given due to physiochemical reactions of samples at a specific temperature range and heating rate. These characteristic curves are obtained due to the physical processes occurring in the sample.

In this study, degradation of samples was observed in the temperature range of 0 ^{o}C– 450^{o}C at a heating rate of 10 ^{o}C/min.

4.4.4 X-ray Diffraction (XRD)

In this study, the identification of mineral components of the electrospun mats was achieved by X-ray Diffraction (XRD).

XRD is an analytical technique used to identify unknown crystalline materials. Monochromatic x-ray is used to calculate the interplanar spacing of the material. Samples in powder form are analyzed in the orientation in which crystallographic directions are achieved by the beam. When the interference is observed, a reflection is produced. The

relative peak height is proportional to the number of grains contained in the powder sample. The x-ray spectra generated in XRD provide a structural fingerprint of the unknown sample. In case of the samples composed of mixtures of crystalline can be analyzed in the same manner. The relative peak heights of the materials can be used for semi-quantitative estimates for the abundance. The x-ray beam is also used to examine the structural information of the thin films on surfaces.

The advantages of analysis using XRD are its rapid identification of materials, ease of sample preparation, large library of known crystalline structures, and computer-aided material identification.

Measurement Conditions:

In this study, the XRD was conducted with the following instrument settings:

For pure HA powder:

Start Position [°2Th.]	15.0100
End Position [°2Th.]	119.9900
Step Size [°2Th.]	0.0200
Scan Step Time [s]	0.5000

For HA-polymer electrospun mats:

Start Position [°2Th.]	20.0100
End Position [°2Th.]	69.9900
Step Size [°2Th.]	0.0200
Scan Step Time [s]	4.3000

The following parameters were kept constant for both HA powder and HA-polymer electrospun mats:

Scan Type	Continuous
Offset [°2Th.]	0.0000
Divergence Slit Type	Fixed
Divergence Slit Size [°]	0.8709
Specimen Length [mm]	10.00
Receiving Slit Size [mm]	0.1000
Measurement Temperature [°C]	25.00
Anode Material	Cu
Generator Settings	45 kV, 40 mA
Goniometer Radius [mm]	200.00
Dist. Focus-Diverg. Slit [mm]	100.00
Incident Beam Monochromator	No
Spinning	No

CHAPTER 5

RESULTS

The HA-polymer solution prepared in method 1 developed a number of lumps of HA particles due to the overnight stirring of HA powder in polymer solution. The resulting electrospun mats contained large lumps of HA powder which are not desirable for ideal scaffold. For this reason, the method 1 was not successful. On the contrary, the HA-polymer solution prepared in method 2 did not develop HA lumps and the resulting electrospun mat did not contain distinctive lumps of HA powder.

In the biomimetic procedure of electrospun mats treated with SBF, all the electrospun mats shrank after they were immersed in an aqueous suspension of 0.2 wt% calcium hydroxide at 40 ℃ for 24 hours being shaken at a rate of 60 times/min. All the PLGA SF mats were completely dissolved, the PLLA SF mats shrank to about 50% of their original size, the PLLA LF and PLGA LF shrank to about 60~70% of their original size. For this reason, the biomimetic procedure was not successful for this study and the characterization for the scaffold developed by this procedure is not included in this section.

5.1 Morphology and Elemental Composition of HA and Electrospun Scaffold

The morphology of HA powder was observed under scanning electron microscope (SEM). The original HA crystals have a mean diameter in the range of 20 ~ 30 μ m (Figure 5.1, 5.2). The HA powder ground before the addition to the polymer solution was also observed under SEM and showed a mean diameter size in the range of 3 ~ 8 μ m

(Figure 5.3). EDXA of ground HA powder indicates the quantitative result of each element contained in HA in weight % and atomic % (Figure 5.4). The weight % ratio of P/Ca in EDXA result showed to be 1.85 which is very close to the elemental weight % ratio of P/CA=2.16 of HA, confirming the stoichiometry of HA.

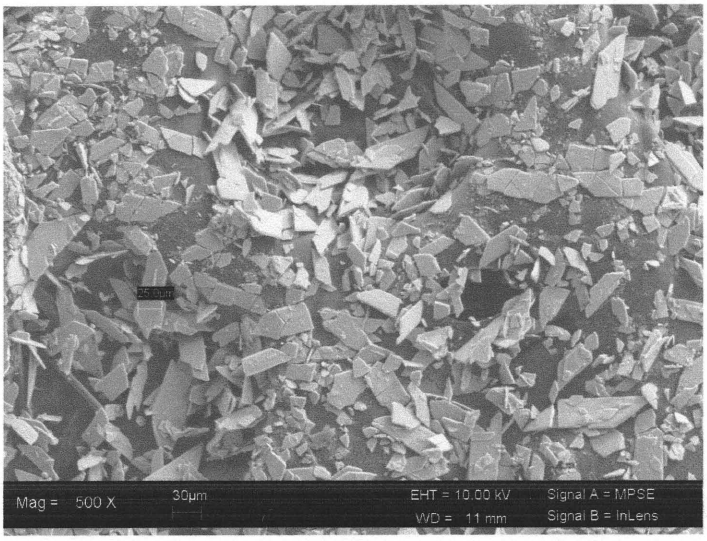

Figure 5.1 Pure HA crystals at 500X magnification.

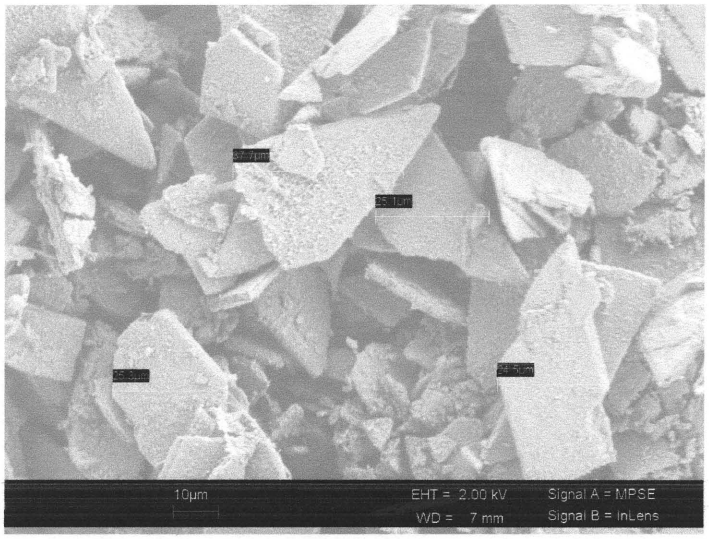

Figure 5.2 Pure HA crystals at 2.25kX magnification.

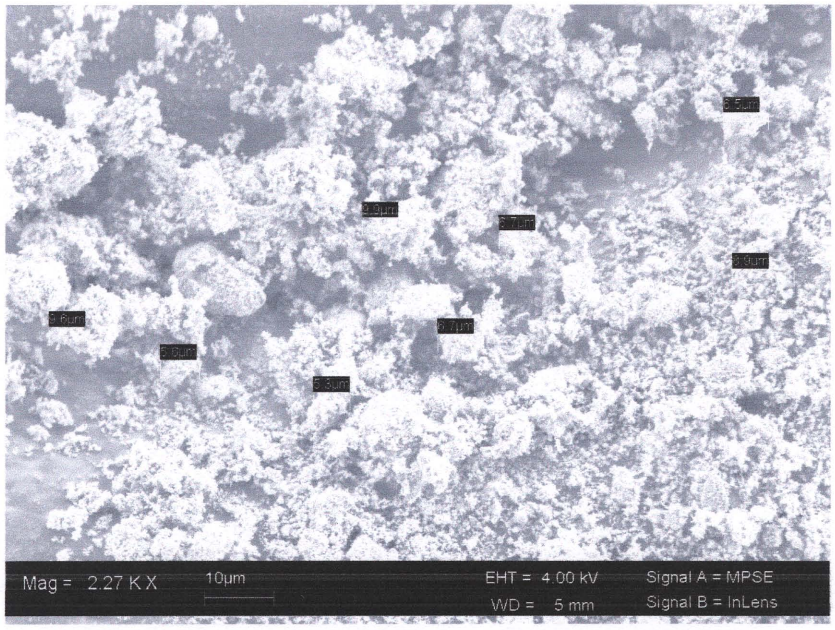

Figure 5.3 Ground HA powder at 2.27 KX magnification.

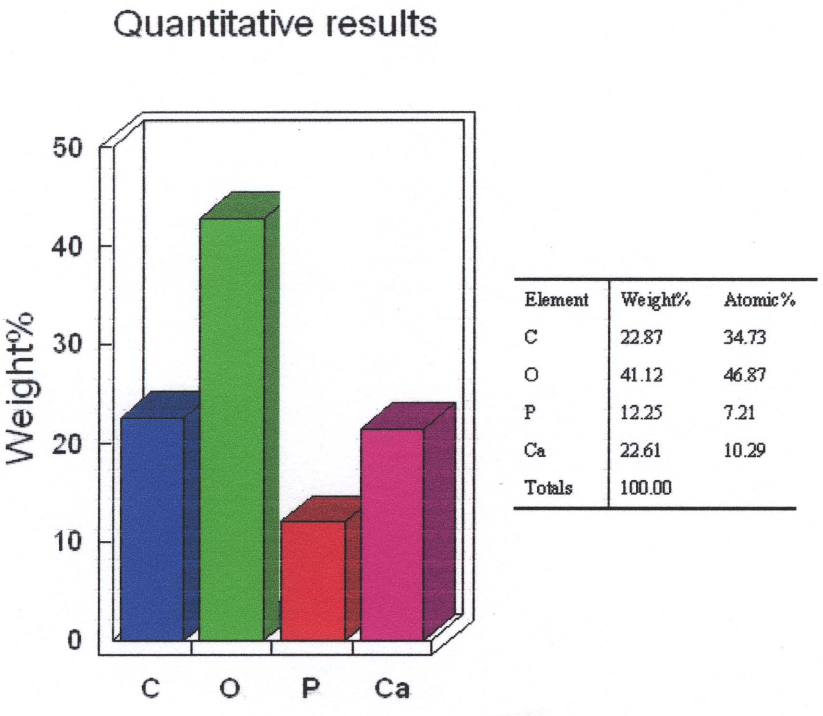

Element	Weight%	Atomic%
C	22.87	34.73
O	41.12	46.87
P	12.25	7.21
Ca	22.61	10.29
Totals	100.00	

Figure 5.4 EDXA of ground HA powder at 500X.

The electrospun pure PLLA LF mat was observed under SEM at 500X magnification following carbon coating (Figure 5.5). The result of EDXA showed the elemental composition of pure PLLA polymer; carbon 77.98 wt%, oxygen 22.00 wt%, phosphorus 0.01 wt%, and calcium 0.05 wt%, confirming that pure polymer did not contain any phosphorus or calcium (Figure 5.6).

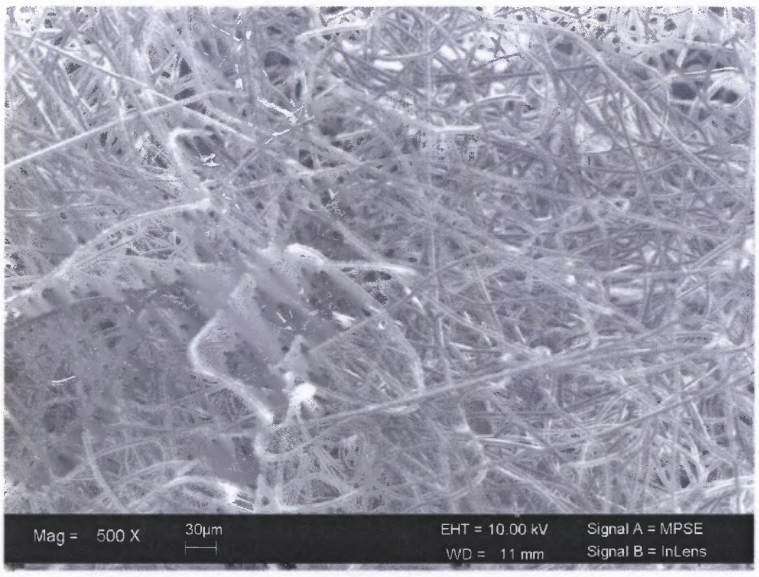

Figure 5.5 PLLA LF pure electrospun mat (0% HA) at 500X magnification.

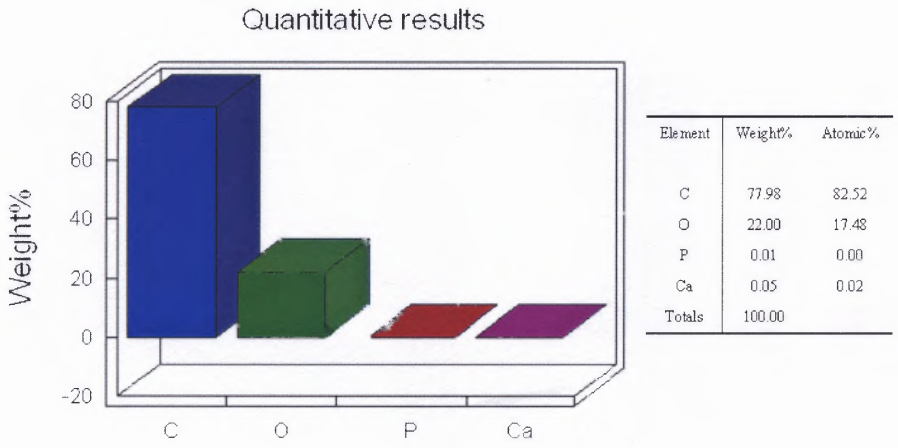

Figure 5.6 EDXA of Pure PLLA LF mat at 500X.

The electrospun PLLA LF 10% HA mat was observed under SEM at 500X and 2.25 KX magnification following carbon coating (Figures 5.7, 5.8). The image at 2.25 KX magnification showed HA particles in the polymer fiber (Figure 5.8). The size of HA particles is in the range of 1.6 ~ 3.3 μ m. The result of EDXA at 500 X showed the elemental composition of PLLA LF 10% HA and the wt% of calcium was slightly higher than that of pure PLLA (Figure 5.9).

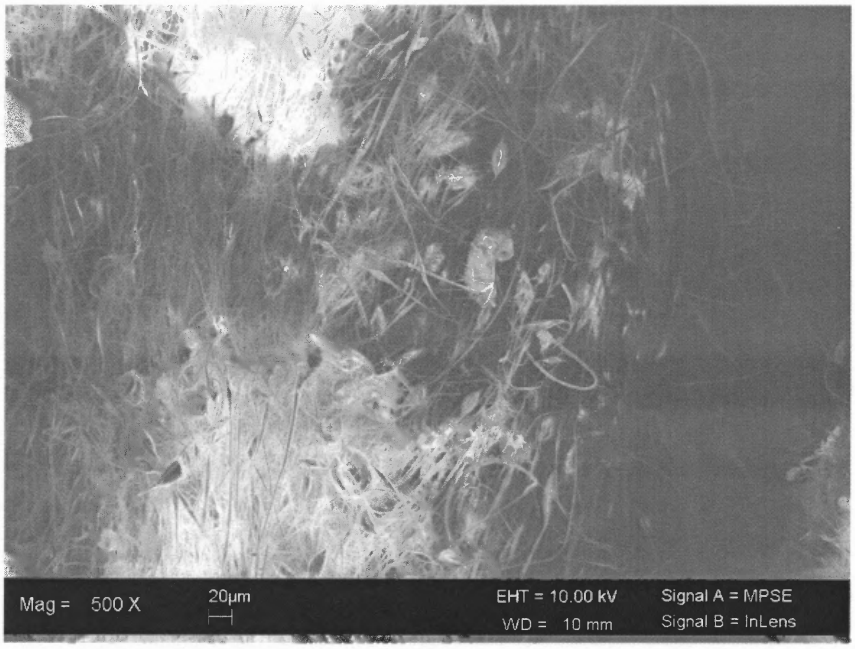

Figure 5.7 PLLA LF 10% HA electrospun mat at 500X magnification.

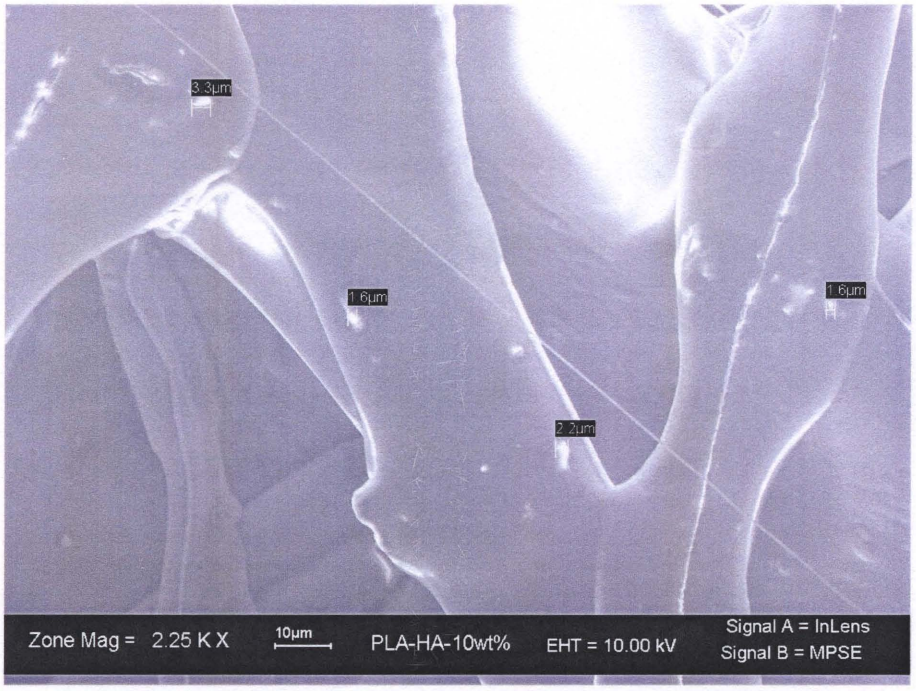

Figure 5.8 PLLA LF 10% HA electrospun mat at 2.25KX magnification.

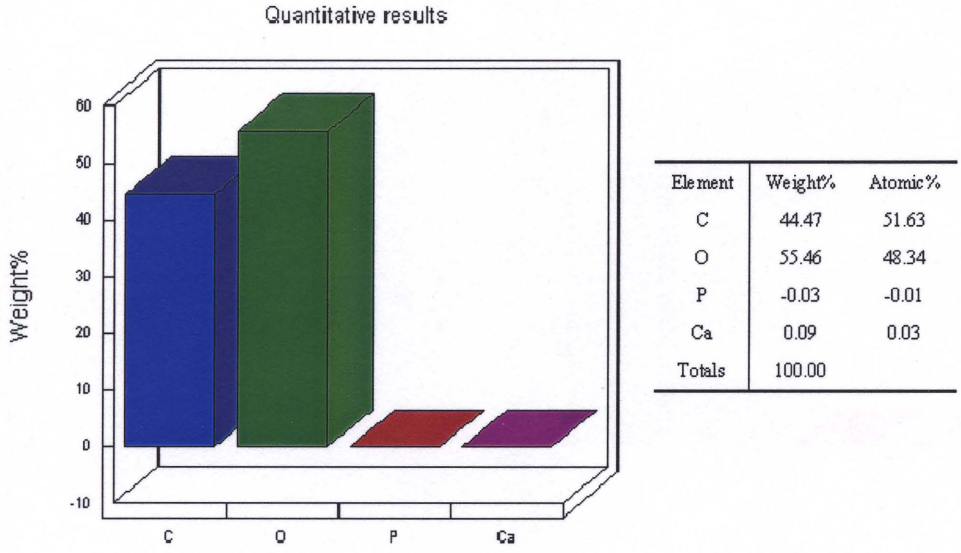

Element	Weight%	Atomic%
C	44.47	51.63
O	55.46	48.34
P	-0.03	-0.01
Ca	0.09	0.03
Totals	100.00	

Figure 5.9 EDXA of PLLA LF 10% HA electrospun mat at 500X.

The electrospun PLLA LF 25% HA mat was observed under SEM at 500X and 2.25 KX magnification following carbon coating (Figures 5.10, 5.11). The image at 2.25 KX magnification showed the HA particles in the polymer fiber (Figure 5.11). The size of HA particles is in the range of 2.2 ~ 6.2 μ m. The result of EDXA at 500X showed the elemental composition of both calcium and phosphorus of PLLA LF 25% HA was higher than that of pure PLLA (Figure 5.12).

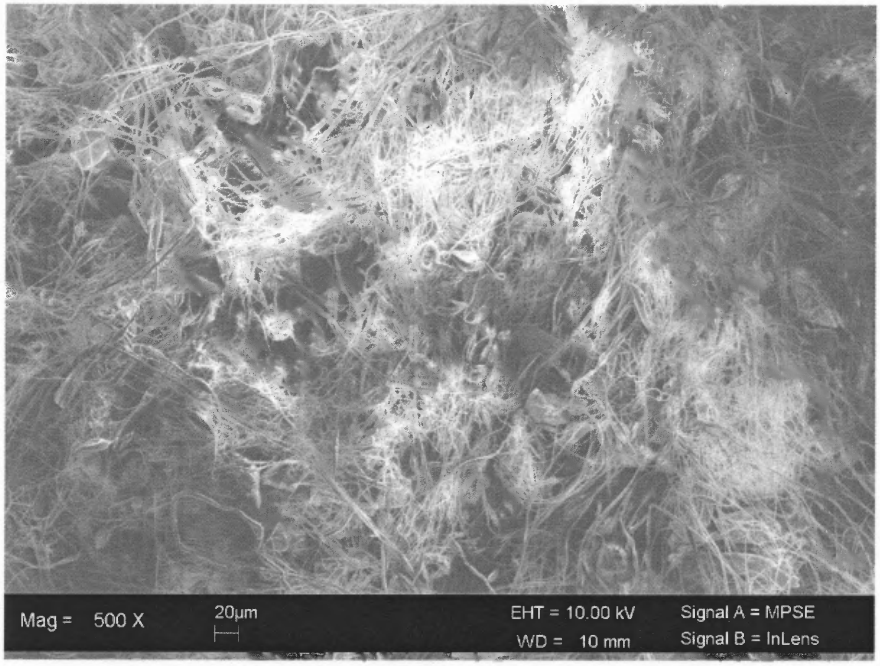

Figure 5.10 PLLA LF 25% HA electrospun mat at 500X magnification.

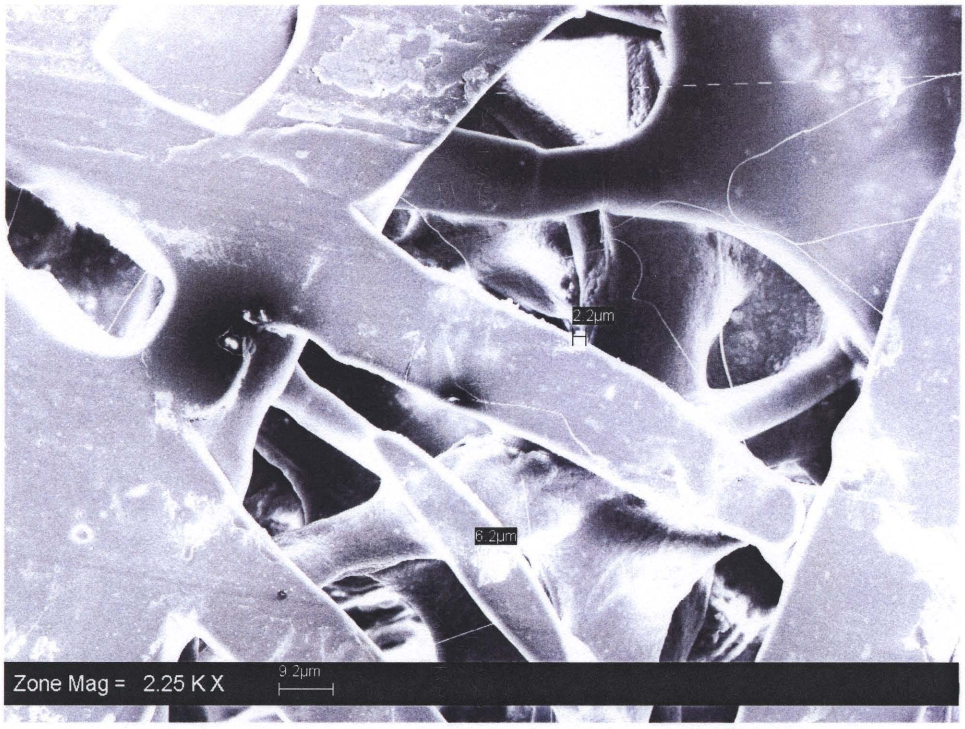

Figure 5.11 PLLA LF 25% HA electrospun mat at 2.25KX magnification.

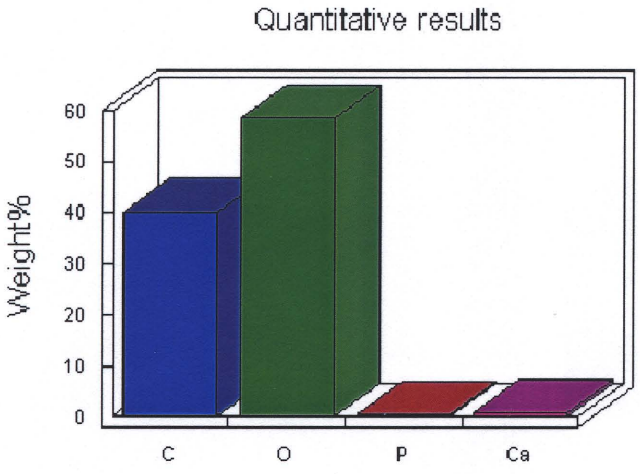

Element	Weight%	Atomic%
C	40.24	47.55
O	58.61	51.99
Na	0.06	0.04
P	0.35	0.16
Ca	0.75	0.26
Totals	100.00	

Figure 5.12 EDXA of PLLA LF 25% HA electrospun mat at 500X.

The electrospun pure PLGA LF mat was observed under SEM at 500X and 2.25 KX magnification following carbon coating (Figures 5.13, 5.14). The result of EDXA showed the elemental composition of pure PLGA polymer; carbon 40.62 wt%, oxygen 59.41 wt%, phosphorus 0.02 wt%, and calcium -0.13 wt%, confirming that pure polymer did not contain any phosphorus or calcium (Figure 5.14).

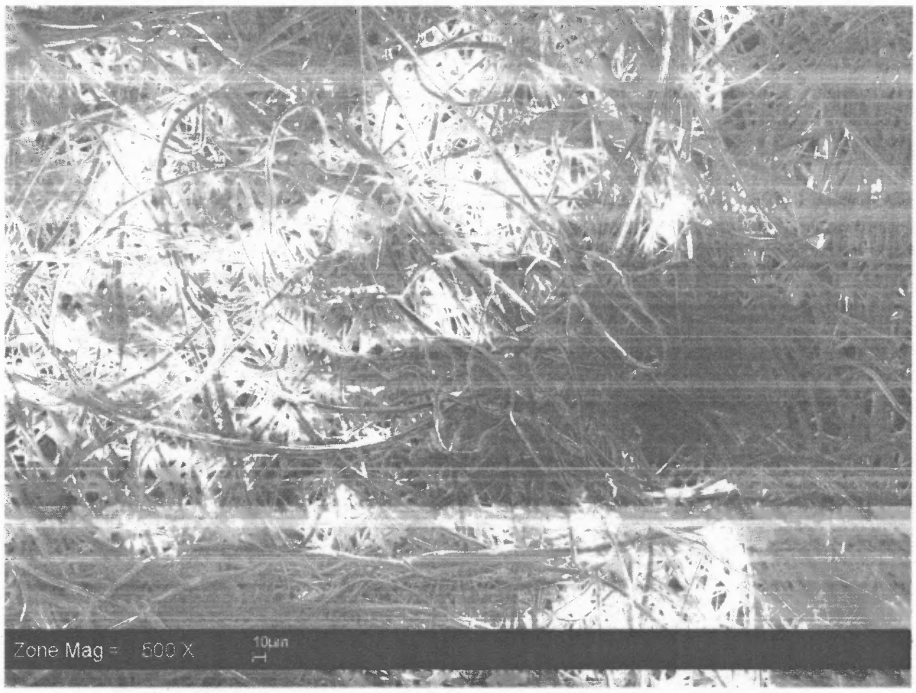

Figure 5.13 PLGA LF pure electrospun mat (0% HA) at 500X magnification.

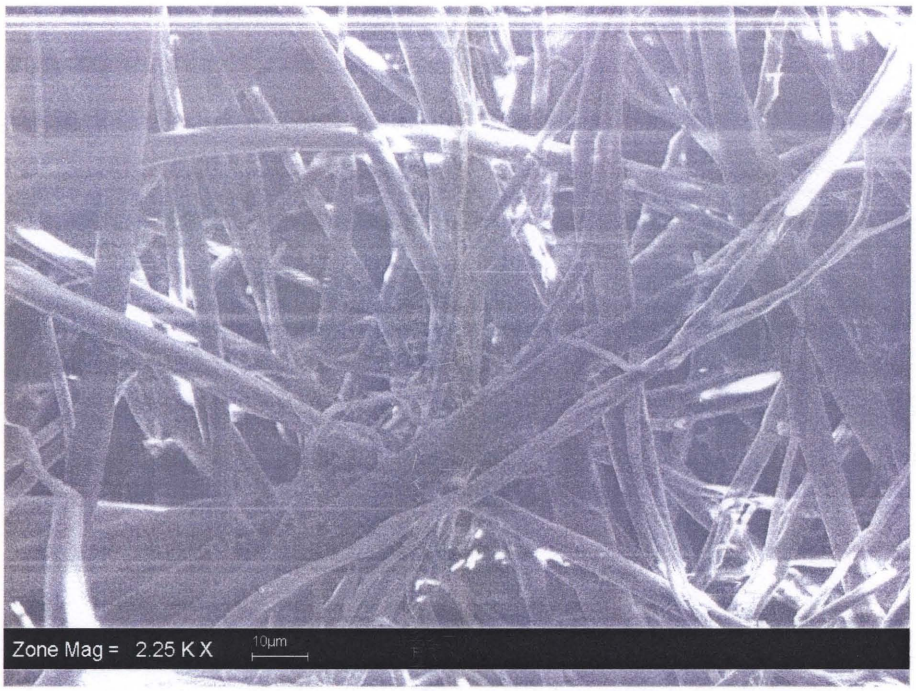

Figure 5.14 PLGA LF pure electrospun mat (0% HA) at 2.25 KX magnification.

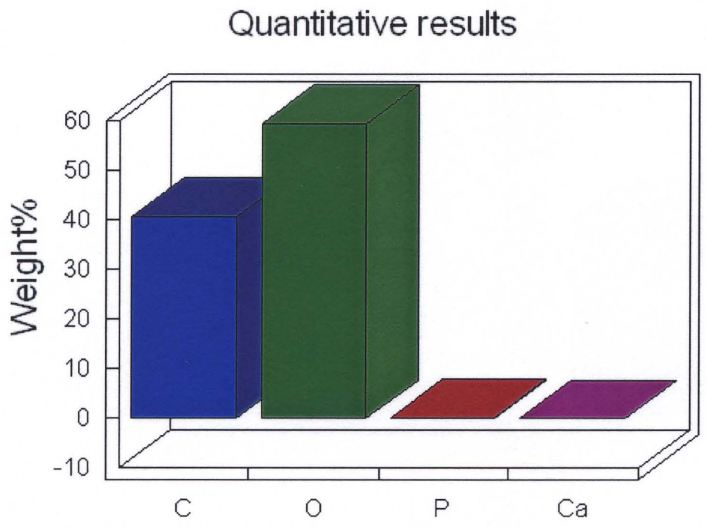

Element	Weight%	Atomic%
C	40.62	47.66
O	59.41	52.33
P	0.02	0.01
Ca	-0.13	-0.05
Totals	100.00	

Figure 5.15 EDXA PLGA LF at 500X.

The electrospun PLGA LF 10% HA mat was observed under SEM at 500X and 2.25 KX magnification following the carbon coating (Figures 5.16, 5.17). The image at 2.25 KX magnification showed the HA particles in the polymer fiber (Figure 5.17). The size of HA particles is in the range of 2.9 ~ 10.0 μ m. The result of EDXA at 500X showed the elemental composition of PLGA LF 10% HA and the presence of calcium and phosphorus were not confirmed (Figure 5.18).

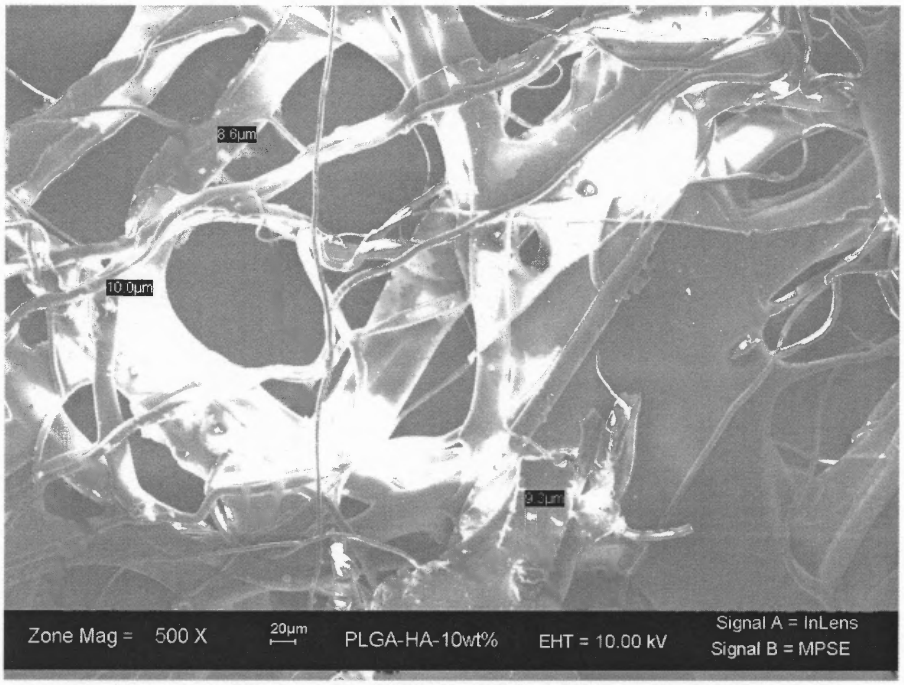

Figure 5.16 PLGA LF 10% HA electrospun mat at 500X magnification.

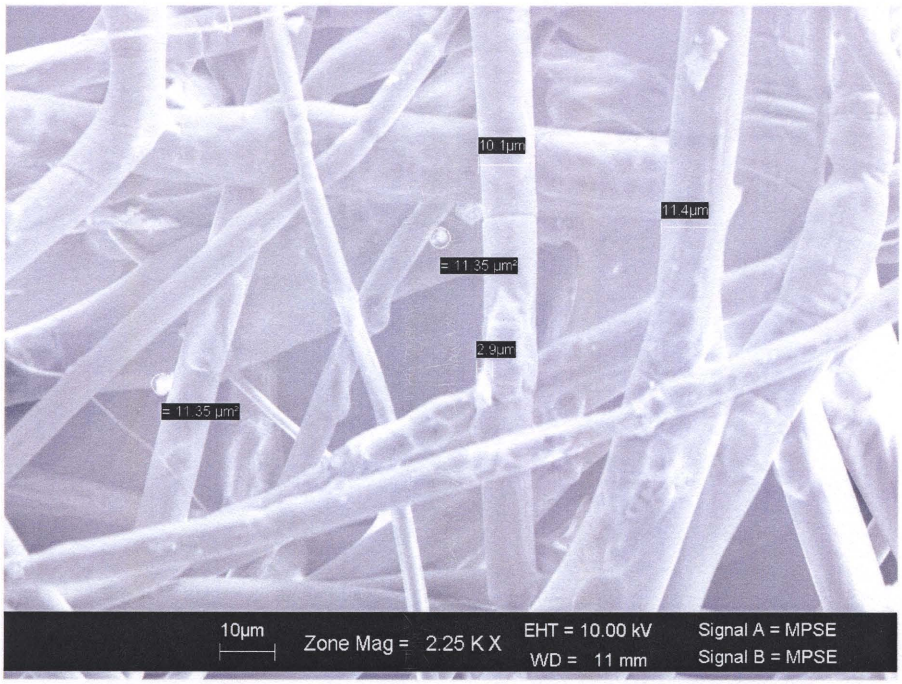

Figure 5.17 PLGA LF 10% HA electrospun mat at 2.25 KX magnification.

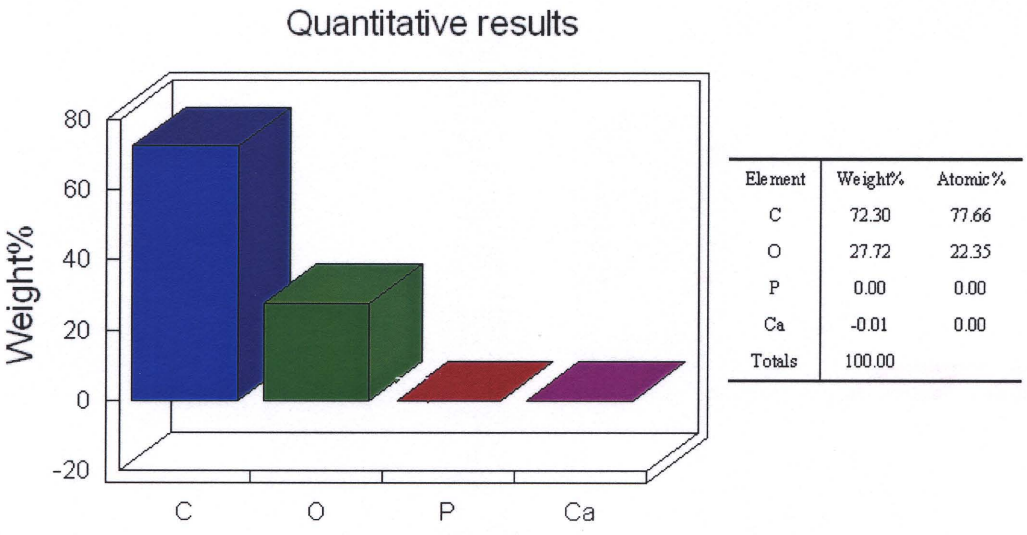

Element	Weight%	Atomic%
C	72.30	77.66
O	27.72	22.35
P	0.00	0.00
Ca	-0.01	0.00
Totals	100.00	

Figure 5.18 EDXA of PLGA LF 10% HA electrospun mat at 500X.

The electrospun PLGA LF 25% HA mat was observed under SEM at 500X and 2.25 KX magnification following the carbon coating (Figures 5.19, 5.20). The image at 2.25 KX magnification showed the HA particles in the polymer fiber (Figure 5.20). The size of HA particles is in the range of 2.5 ~ 7.1 μ m. The result of EDXA at 500X showed the elemental composition of both calcium and phosphorus of PLGA LF 25% HA was higher than that of pure PLLA (Figure 5.21).

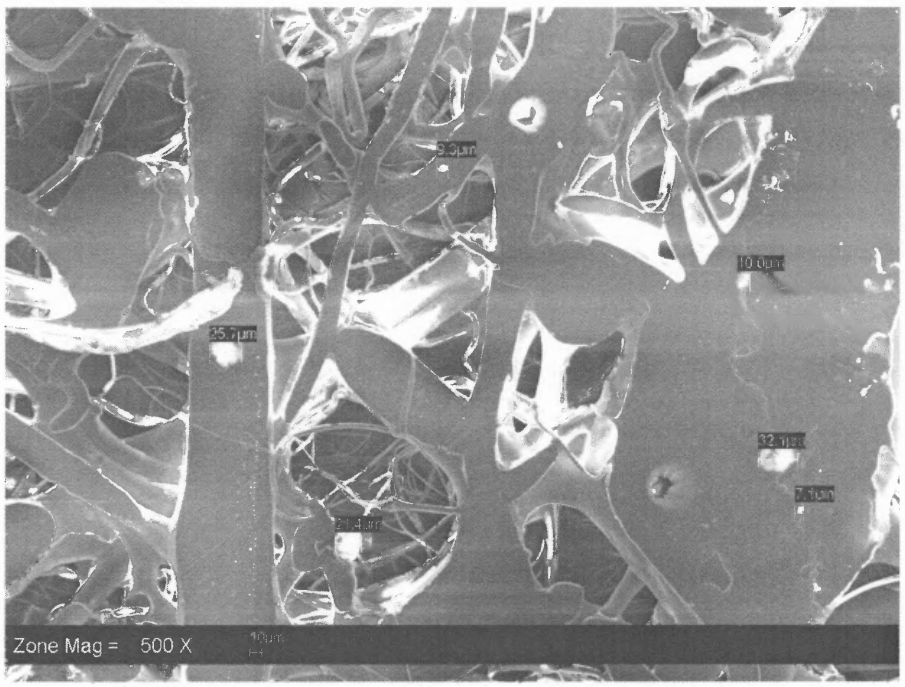

Figure 5.19 PLGA LF 25% HA electrospun mat at 500X magnification.

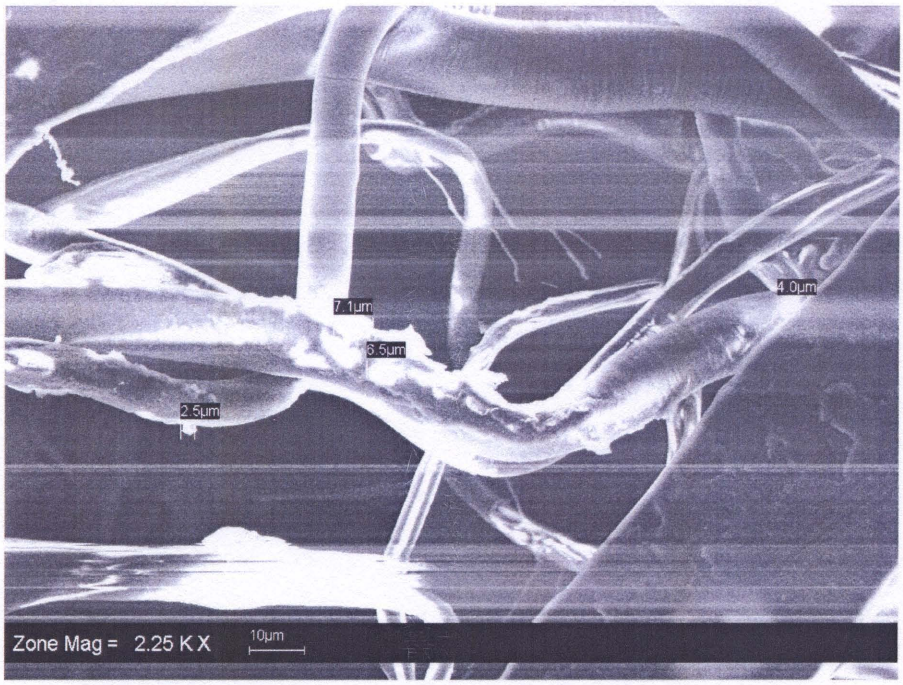

Figure 5.20 PLGA LF 25% HA electrospun mat at 2.25 KX magnification.

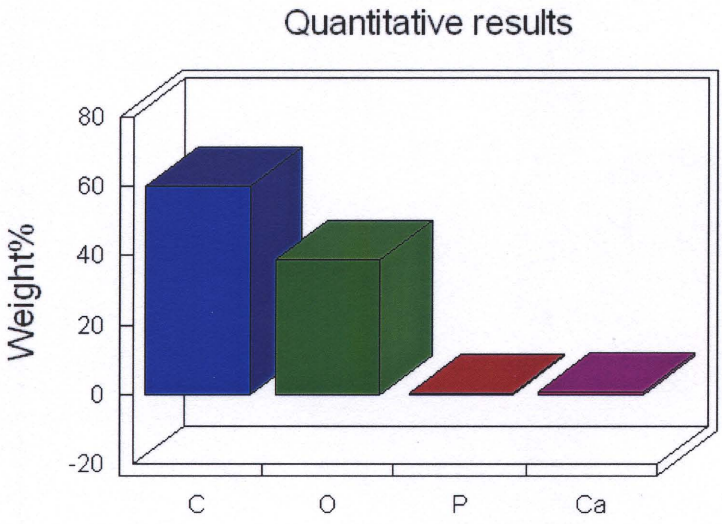

Element	Weight%	Atomic%
C	60.04	67.01
O	38.91	32.61
P	0.28	0.12
Ca	0.78	0.26
Totals	100.00	

Figure 5.21 EDXA of PLGA LF 25% HA electrospun mat at 500X.

5.2 Thermal Gravimetric Analysis (TGA)

Thermal gravimetric analysis (TGA) was carried out using Q50 Thermogravimetric Analyzer. TGA was used to observe the temperature dependent weight changes in the HA incorporated electrospun mats. In this analysis, the heating was carried out in the range of 0 °C to 450 °C at the rate of 10 °C per minute for all the samples. All the TGA figures are shown in Appendix B.

The TGA was conducted on pure HA powder, and pure polymer electrospun mats, PLLA LF, PLLA SF, PLGA LF, and PLGA SF, as references (Figure B.1 - B.5). The pure HA powder showed 97.40 % weight retention confirming that HA powder was not affected at the temperature range of 0 °C to 450 °C (Figure B.1). On the contrary, all the weight retention percentages of the pure polymer electrospun mats were under one percent at 450 °C; PLLA LF – 0.2653%, PLLA SF – 0.6026%, PLGA LF – 0.9221%, and PLGA SF – 0.6447% (Figure B.2 – B.5). This result indicates that all the pure polymers went through decomposition process before the temperature reached to 450 °C. Thus the weight retention of each sample containing HA at 450 °C is considered as weight percent deposits of HA powder.

The TGA was conducted twice on each HA incorporated electrospun mats. Two samples were randomly selected from each electrospun mat and cut out for TGA.

The first TGA data for PLLA-HA and PLGA-HA are shown in Table 5.1 and Table 5.3, respectively. The second TGA data for PLLA-HA and PLGA-HA are shown in Table 5.2, and Table 5.4, respectively. The average weight percent of HA deposits of each mat was calculated and shown in Table 5.5, Table 5.6, and Figure 5.22.

Table 5.1 Weight Retention of PLLA/HA Electrospun Mats 1st Run

	LF 0% HA	SF 0% HA	LF 10% HA	SF 10% HA	LF 25% HA	SF 25% HA
Wt% HA at 450 °C	0.2653	0.6024	7.224	7.816	18.36	20.31

Table 5.2 Weight Retention of PLLA/HA Electrospun Mats 2nd Run

	LF 0% HA	SF 0% HA	LF 10% HA	SF 10% HA	LF 25% HA	SF 25% HA
Wt% HA at 450 °C	0.2653	0.6024	11.69	8.996	21.82	20.3

Table 5.3 Weight Retention of PLGA/HA Electrospun Mats 1st Run

	LF 0% HA	SF 0% HA	LF 10% HA	SF 10% HA	LF 25% HA	SF 25% HA
Wt% HA at 450 °C	0.9221	0.6447	7.542	9.544	12.48	20.14

Table 5.4 Weight Retention of PLGA/HA Electrospun Mats 2nd Run

	LF 0% HA	SF 0% HA	LF 10% HA	SF 10% HA	LF 25% HA	SF 25% HA
Wt% HA at 450 °C	0.9221	0.6447	6.683	8.131	19.07	20.05

Table 5.5 Average Weight Retention of PLLA/HA Electrospun Mats

	LF 0% HA	SF 0% HA	LF 10% HA	SF 10% HA	LF 25% HA	SF 25% HA
Wt% HA at 450 °C	0.2653	0.6024	9.457	8.406	20.09	20.305

Table 5.6 Average Weight Retention of PLGA/HA Electrospun Mats

	LF 0% HA	SF 0% HA	LF 10% HA	SF 10% HA	LF 25% HA	SF 25% HA
Wt% HA at 450 °C	0.9221	0.6447	7.1125	8.8375	16.285	20.195

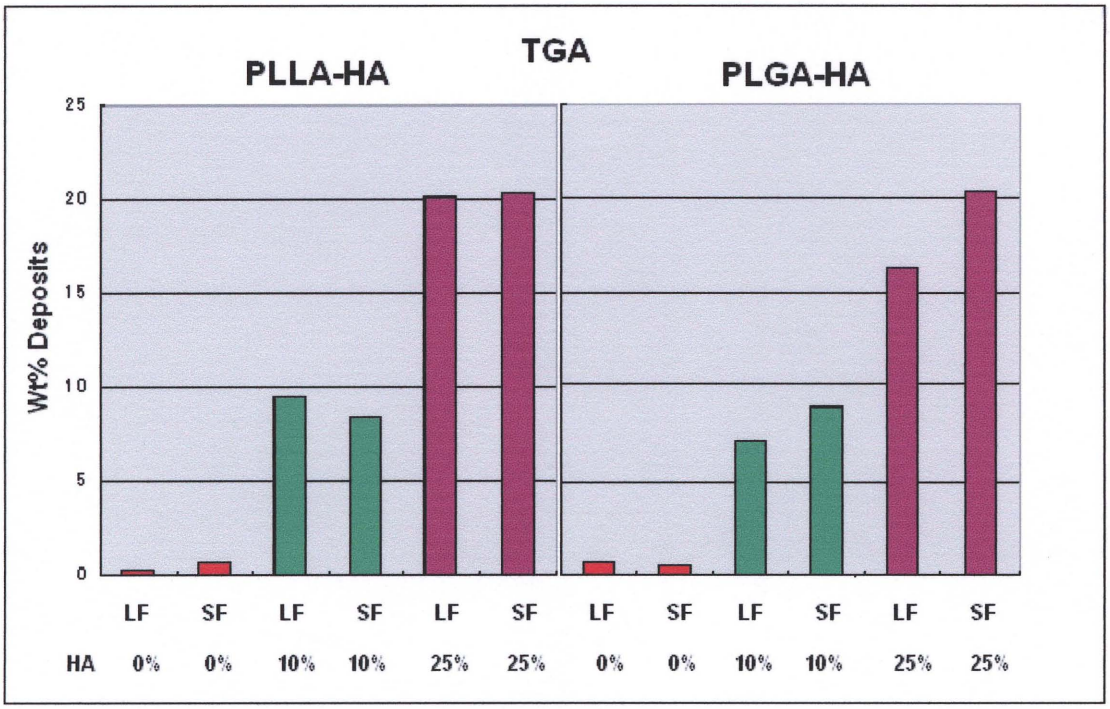

Figure 5.22 The average wt % deposits of HA incorporated PLLA and PLGA electrospun mats.

5.3 X-ray Diffraction (XRD)

The X-ray diffraction (XRD) was conducted on HA incorporated electrospun mats for the material identification. The XRD pattern of pure HA powder was used as a reference for the HA peak at the position of 2theta = 33 (Figure 5.23). The XRD was conducted on PLLA LF 10% HA, PLGA LF 10% HA, PLLA LF 25% HA, and PLGA LF 25% HA samples (Figure 5.24 – 5.27). In all the XRD patterns of the samples, the peaks at the position of 2theta = 33 which corresponds to the HA were observed. This confirms the presence of HA in all the electrospun mats.

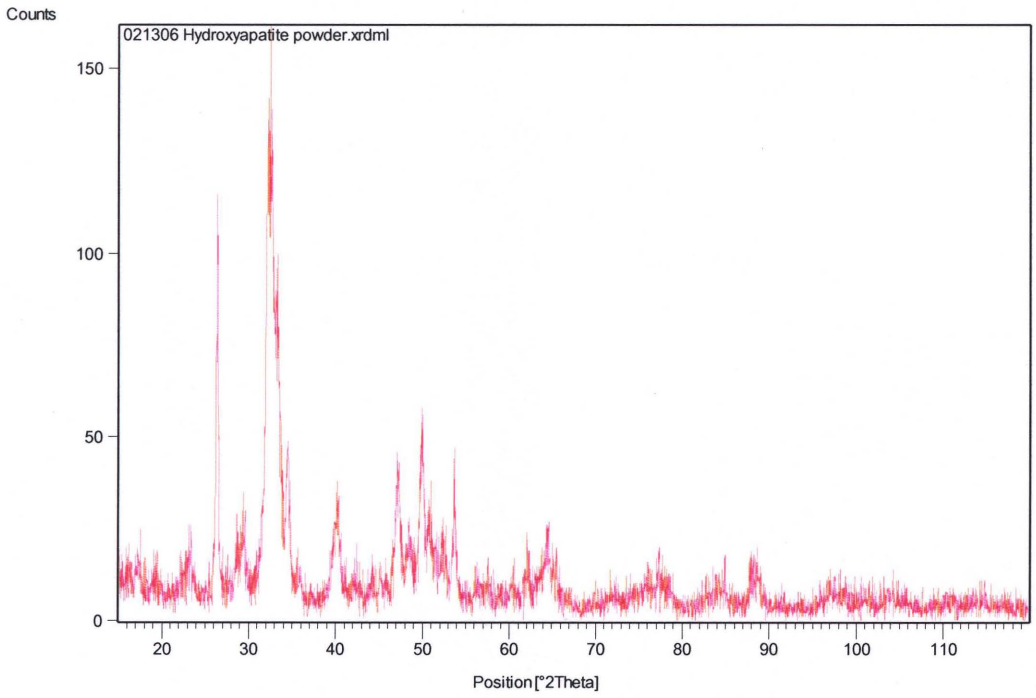

Figure 5.23 XRD of pure HA powder.

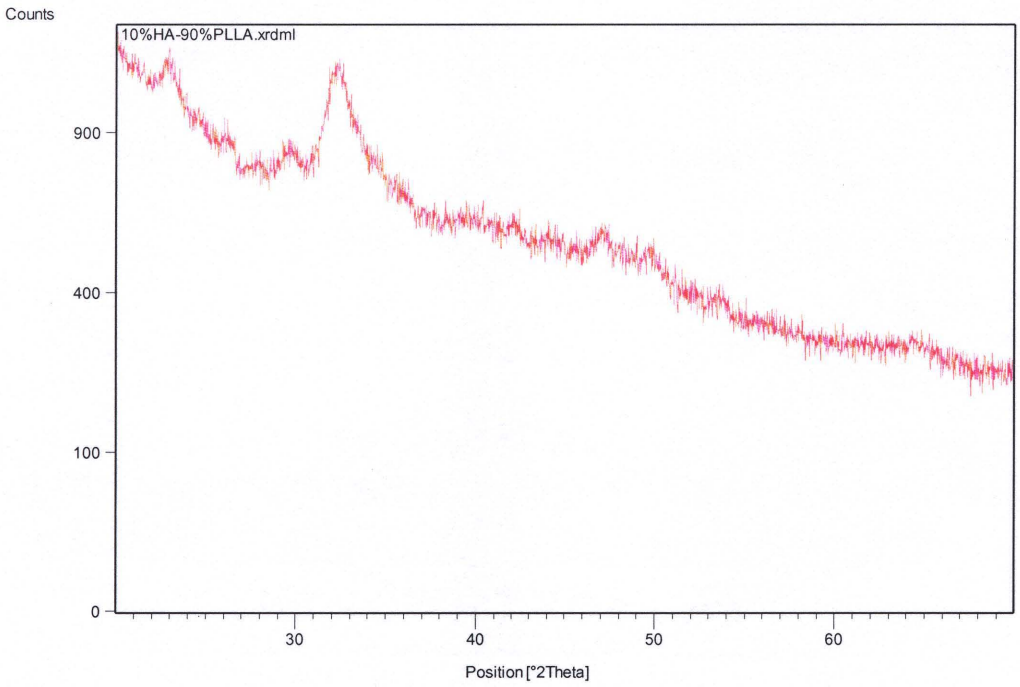

Figure 5.24 XRD of PLLA 10% HA electrospun mat.

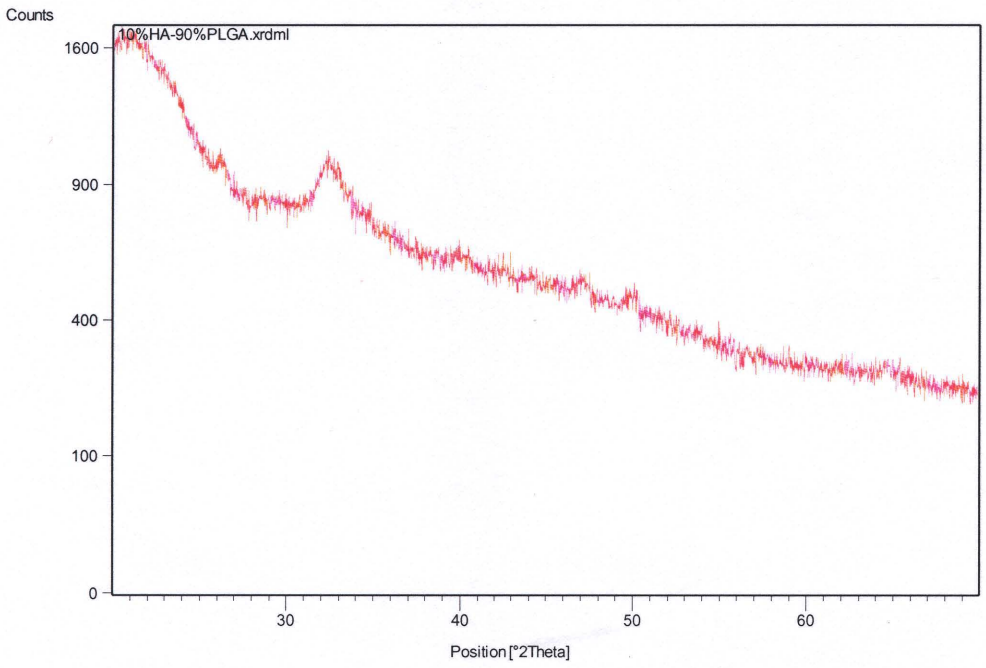

Figure 5.25 XRD of PLGA 10% HA electrospun mat.

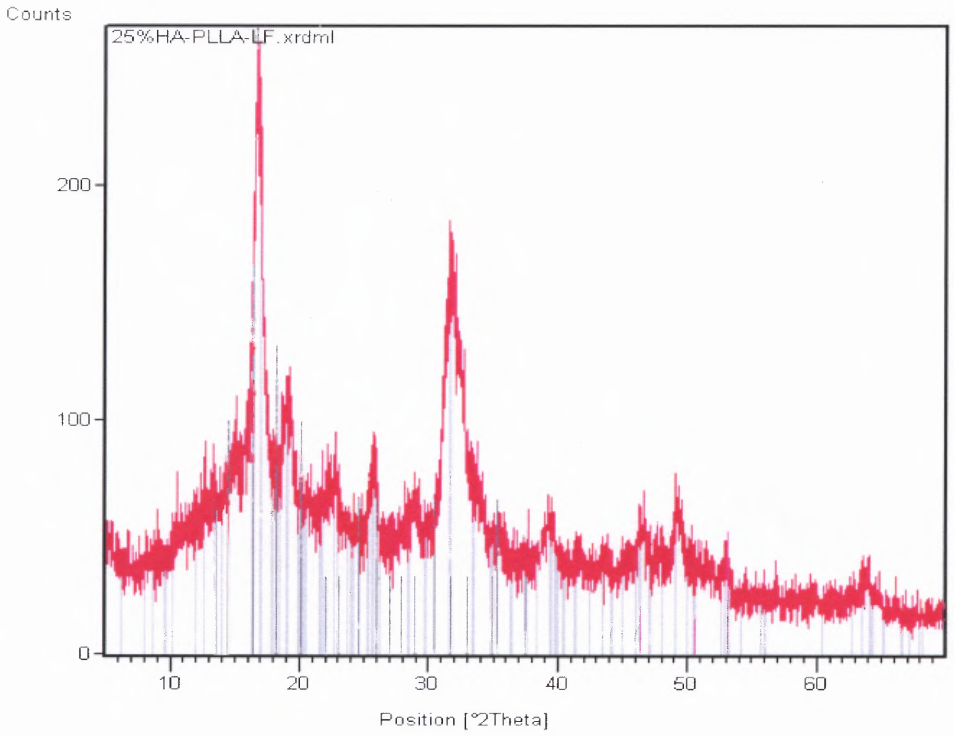

Figure 5.26 XRD of PLLA 25% HA electrospun mat.

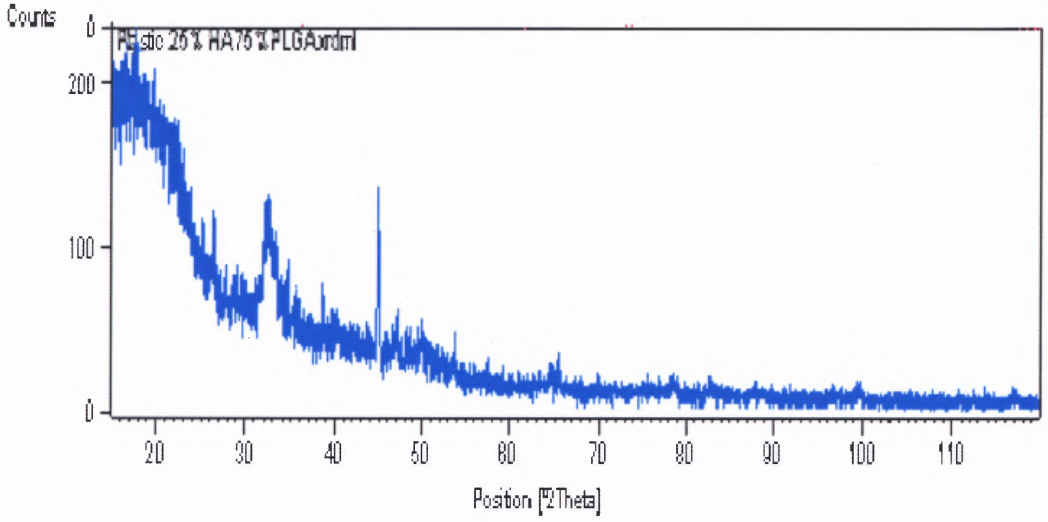

Figure 5.27 XRD of PLGA 25% HA electrospun mat.

CHAPTER 6

CONCLUSION AND DISCUSSION

In this study, hydroxyapatite (HA) particles were successfully incorporated into the three dimensional porous biodegradable PLLA and PLGA polymer fiber mats by electrospinning. The SEM images show the attachment of ground HA particles on the surface of the polymer fibers. The presence of HA in electrospun mats was confirmed by EDXA and XRD. The TGA result showed that the HA incorporated electrospun mats contained HA deposits of 10 – 20% less weight percentage than that of HA originally added in a polymer solution. The possible reason for this loss in weight percentage is that the original HA particles and electrospun samples contained moisture. The moisture contained in the mats was evaporated during the TGA heating process of above 100°C, however, the weight of moisture still contributed for the original weight of the electrospun mats in TGA.

The distinctive difference in properties of electrospun mats developed by large needle (LF) and small needle (SF) was not confirmed in this study. The further characterization and cell study are essential for this evaluation.

The biomimetic process with SBF was also conducted as a secondary approach to produce HA incorporated electrospun mats in this study. This biomimetic approach, however, was not successful since the pure polymer electrospun mats were dissolved when they were treated with calcium hydroxide solution. This may resulted due to the hydrolysis of ester linkage of polymers in the presence of water in calcium hydroxide solution and the hydrolysis of polymers lead the degradation electrospun mats. The hydrolysis reaction might have been accelerated, since the size of the samples punched

out from the electrospun mats was very small and the highly porous structure of electrospun mats increased the exposure of polymer surface to the solution.

Future Recommendations

The testing of mechanical strength and the porosity of the nanofibrous scaffold developed in this study need to be carried out for a complete characterization of the mats. The EDXA is possibly used to analyze the uniformity of dispersion of the HA particles throughout the electrospun mats. The combination with other kind of bioceramics/bioglass such as tricalcium phosphate (TCP) can be used instead of pure HA powder for an optimal induction of bone growth.

After the development of adequate HA incorporated 3-D porous structure is confirmed through characterization, the choice of the desirable cells that interact and expand with the scaffold is the next step. The possible choices of the cells are bone marrow-derived osteoprogenitor cells, osteoblasts, and stem cells for a bone tissue application.

APPENDIX A

PREPARATION OF SBF SOLUTION

SBF is a metastable solution containing calcium and phosphate ions already supersaturated with respect to the apatite. Therefore SBF and 1.5 SBF are prepared as follows using the reagents in Table A.1:

Table A.1 Amounts of Reagents for Preparation of SBF and 1.5 SBF

Reagent	Concentration (mol/m^3)	
	Simulated Body Fluid (SBF) 1000mL	Human Blood Plasma 1000mL
Ultra-pure water	750mL	750mL
NaCl	7.996g	11.994g
$NaHCO_3$	0.350g	0.525g
KCl	0.224g	0.336g
$K_2HPO_4 \cdot 3H_2O$	0.228g	0.342g
$MgCl_2 \cdot 6H_2O$	0.305g	0.458g
1 $kmol/m^3$ HCl	40 cm3	60 cm3
$CaCl_2$	0.278g	0.417g
Na_2SO_4	0.071g	0.107g
$(CH_2OH_3)CNH_2$	6.057g	9.086g
1 $kmol/m^3$ HCl	Appropriate amount for adjusting pH	

(a) Cleaning

- Clean all the bottles including flasks, beakers etc. with dilute hydrochloric acid solution, sterilizing agent and ultra-pure water in this order
- Immerse all the bottles etc. in dilute hydrochloric acid solution for several hours. Remove the bottles from the solution and wash with tap water well.
- Immerse the bottles etc. in sterilizing liquid for overnight. Remove them from the liquid, and washed with ultra-pure water well.
- Wash the bottles with ion-exchanged water for several times and cover their mouths with wrapping film. The bottles do not need to be dried. If the bottles would need to be dried place them in drier below 50 ^{o}C.

(b) Dissolution of chemicals

- Put 750 mL(=cm^3) of ultra-pure water into a 1000 mL beaker (polyethylene beaker is preferred). Stir the water and keep its temperature at 36.5 °C with magnetic stir with heater. The beaker is preferred to be placed in clean bench, to avoid dusts.
- Add each chemical given in Table III into the water until #8, one by one in the order given in Table III, after each reagent was completely dissolved. Weigh a chemical with weighing bottle. Add it in the water. Wash the remaining chemical on the weighing bottle with ultra-pure water and add the solution in the water.
- Addition of reagent #9 should be little by little with less than about 1g, in order to avoid local increase in pH of the solution.

(c) Adjustment of pH

- Calibrate the pH meter with fresh standard buffer solution.
- After #9 on the order in Table III, check the temperature of the solution in the beaker, and place the electrode of pH meter in the solution. Measure its pH while the temperature is at 36.5 °C. At this point, pH of the solution is approximately 7.5. Titrate 1kmol/dm^3-HCl solution with pipette to adjust the pH at 7.25 (or 7.40).
- After the adjustment of pH, transfer the solution from the beaker to a glass volumetric flask of 1000 mL. Wash the inside of the beaker with ultra-pure water several times and add the solution to the flask.
- Add ultra pure water to the solution, adjusting the total volume of the solution to 1000 mL, and the shake the flask well. Keep the flask at room temperature until its temperature should be approximately 20 °C. After cooling, add ultra-pure water again, the solution to the total volume of the solution to 1000 mL, and then shake the flask well.

(d) Storage

- Rinse a polyethylene (or polystyrene) bottle of 1000 mL with a bit of the prepared solution (SBF), at least three times. Transfer the solution from the flask to the polyethylene bottle.
- Store the bottle in a refrigerator at 5-10 °C.

(e) Notes

- Stability of the solution obtained must be examined. Put 50 mL of the solution in a polystyrene bottle and place it in incubator at 36.5 °C. After 2-3 days, check whether the solution has any precipitation or not. If any precipitation would be found, do not use the solution.
- Bottles in which precipitation occur must not be used for any further experiments, because some calcium phosphates would be adhered on their walls inside. A precipitation of calcium phosphate especially such as hydroxyapatite easily induces further formation of hydroxyapatite in the solution, since the simulated body fluid (SBF) is already supersaturated.

APPENDIX B

TERMOGRAVIMETRIC ANALYSIS (TGA)

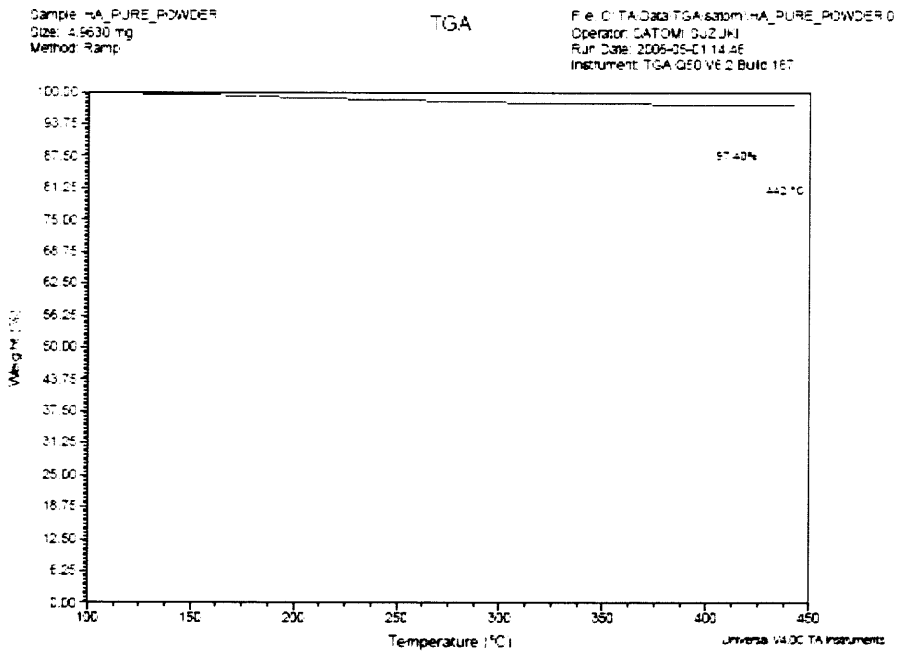

Figure B.1 Percentage weight retention of pure HA powder.

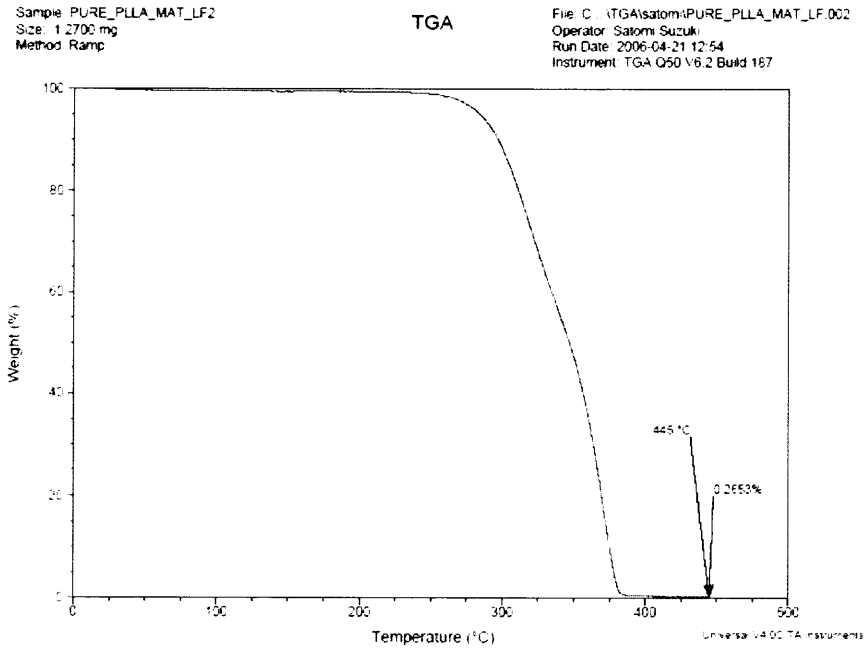

Figure B.2 Percentage weight retention of pure PLLA LF mat.

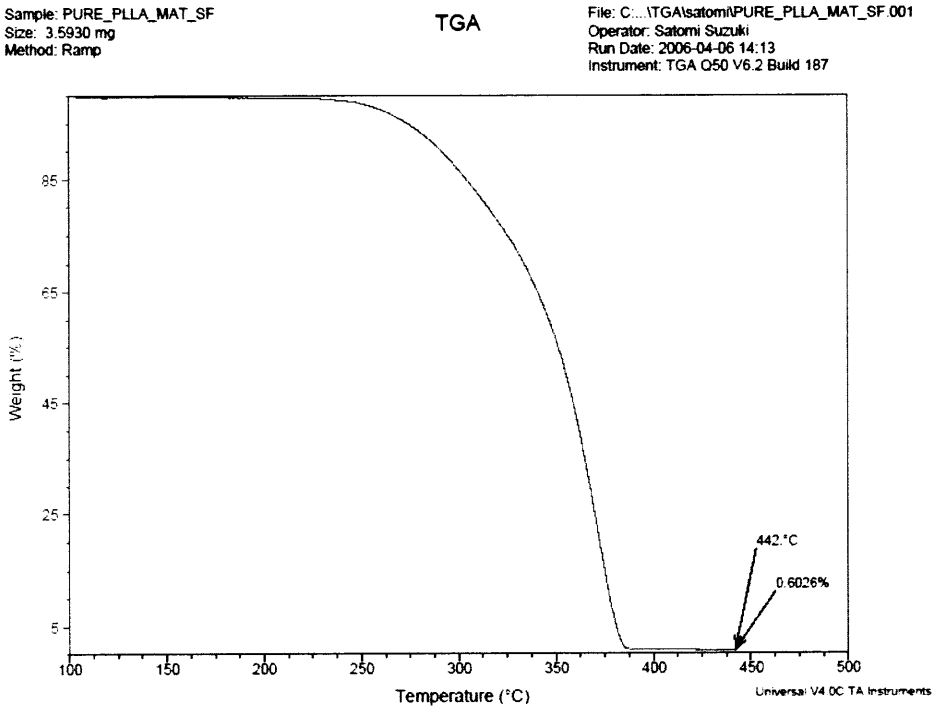

Figure B.3 Percentage weight retention of pure PLLA SF mat.

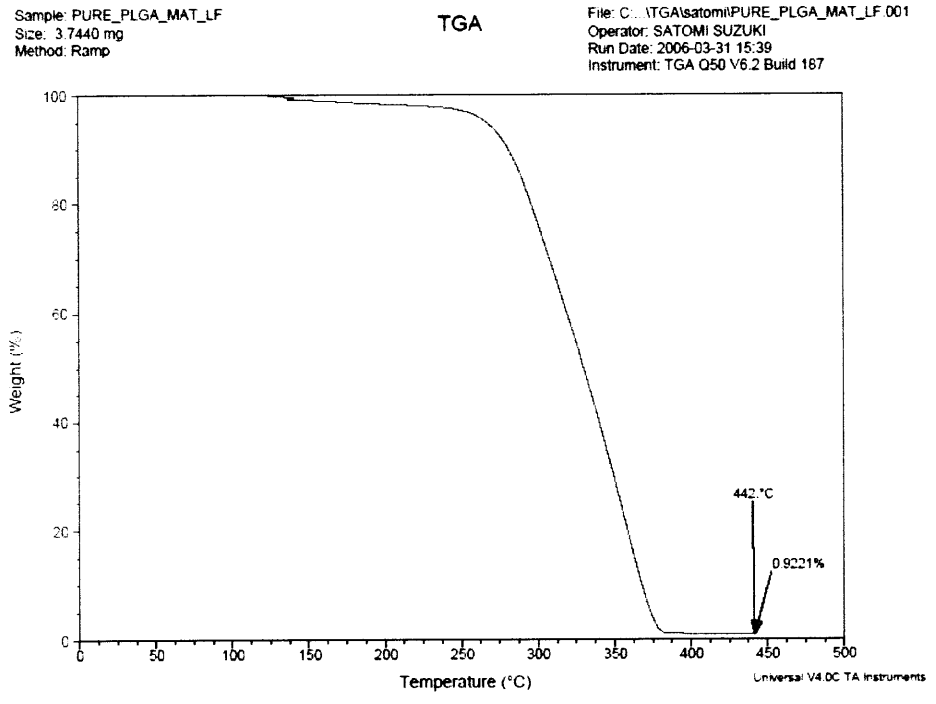

Figure B.4 Percentage weight retention of pure PLGA LF mat.

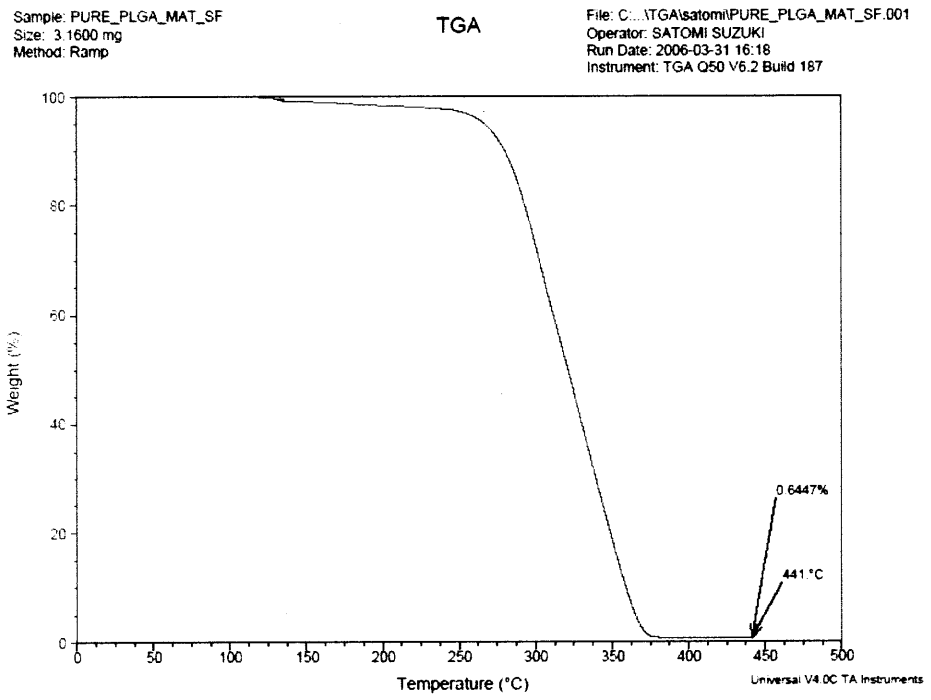

Figure B.5 Percentage weight retention of pure PLGA SF mat.

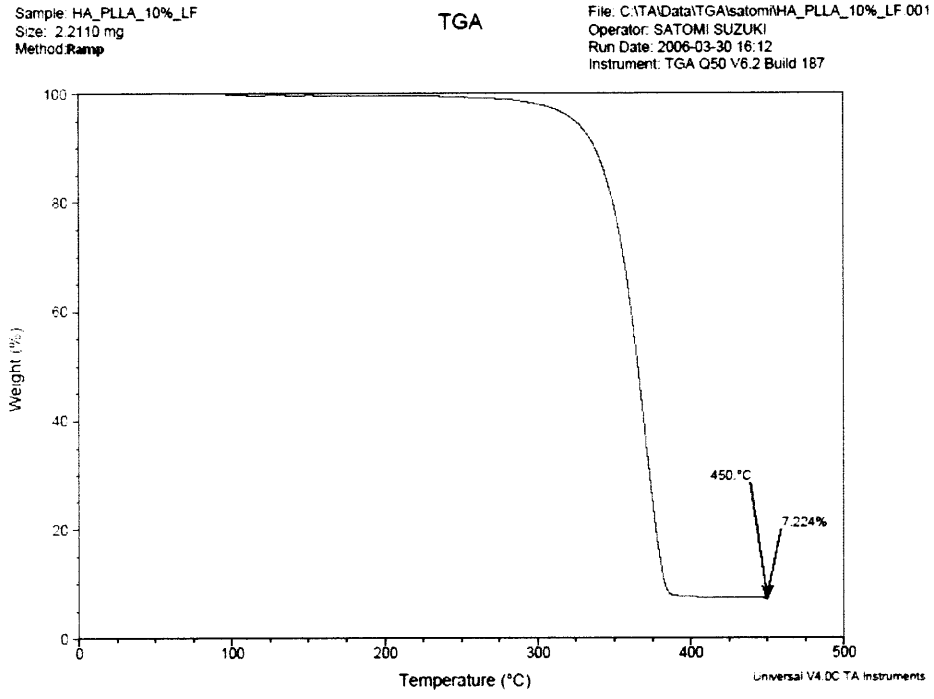

Figure B.6 Percentage weight retention of pure PLLA LF - 10% HA mat.

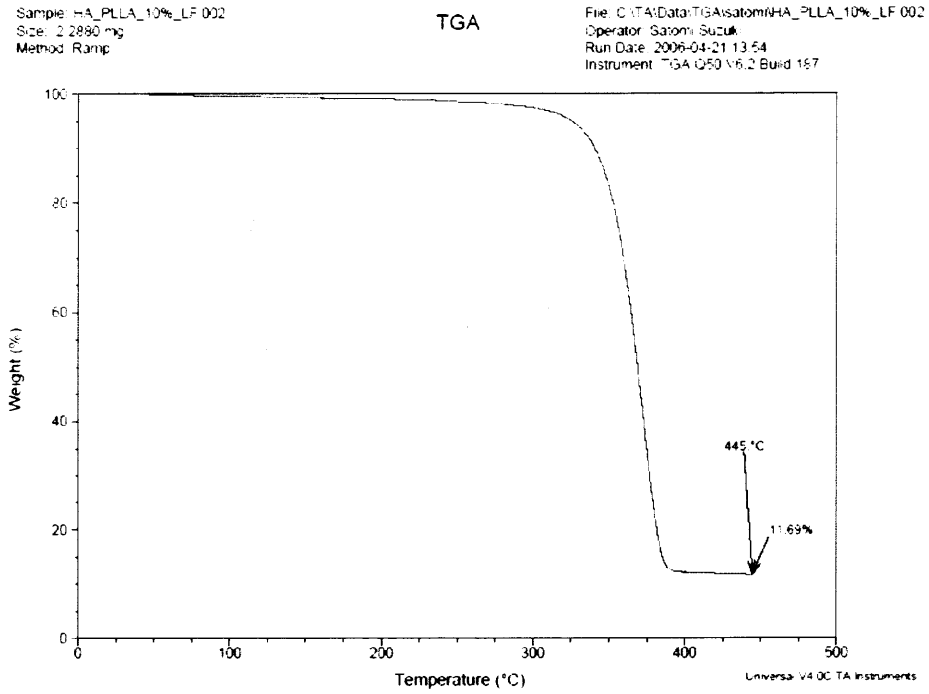

Figure B.7 Percentage weight retention of pure PLLA LF - 10% HA mat.

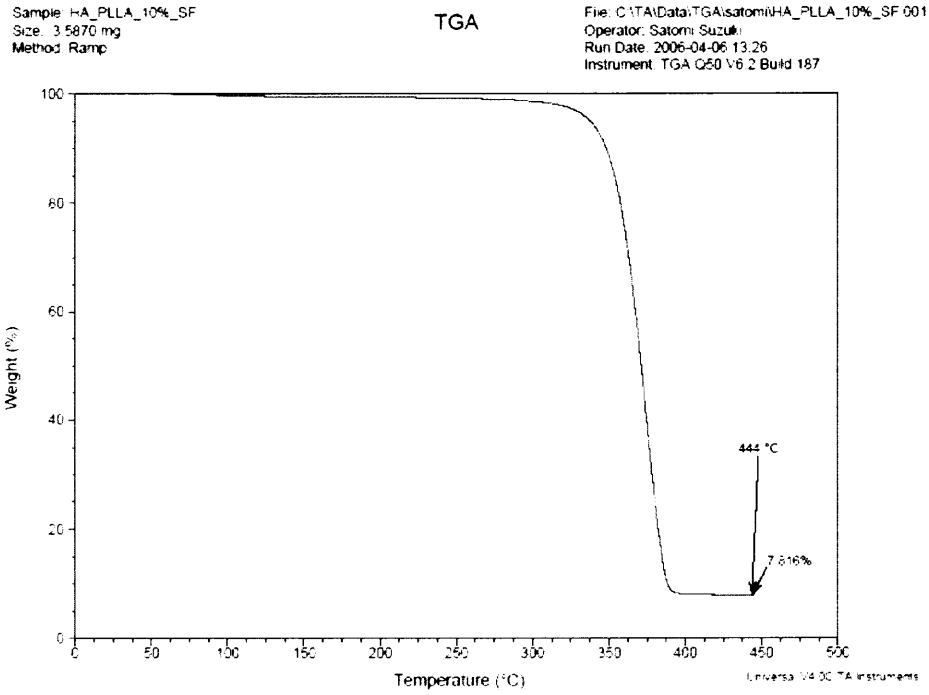

Figure B.8 Percentage weight retention of pure PLLA SF - 10% HA mat.

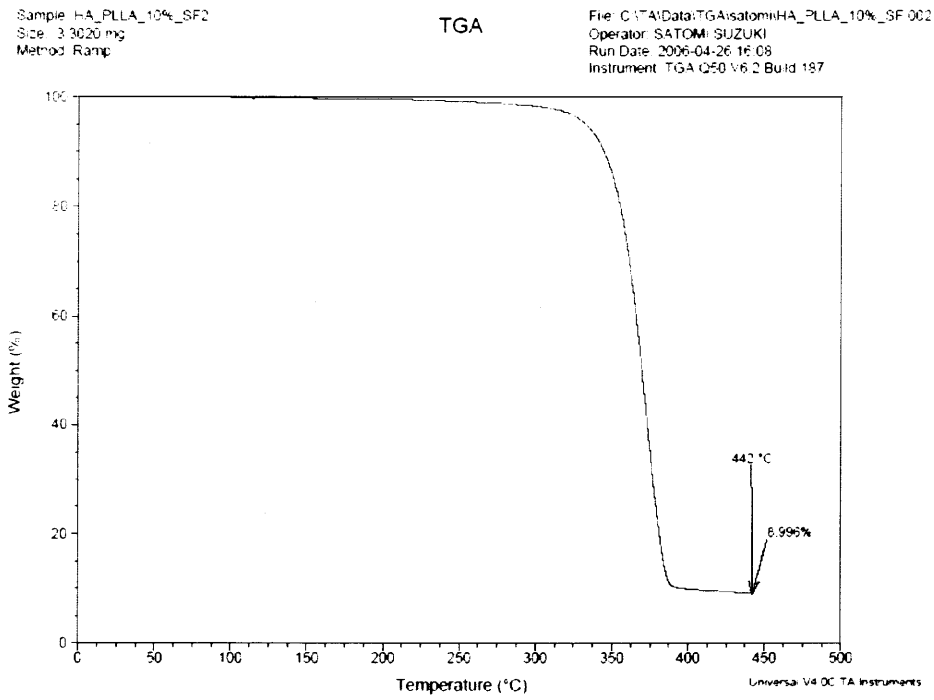

Figure B.9 Percentage weight retention of pure PLLA SF - 10% HA mat.

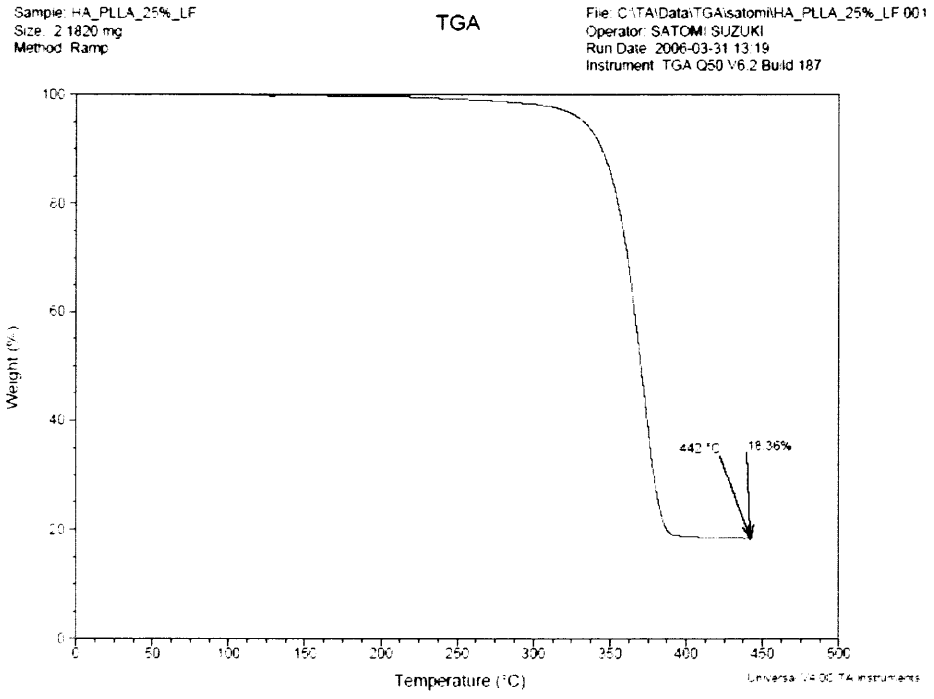

Figure B.10 Percentage weight retention of pure PLLA LF - 25% HA mat.

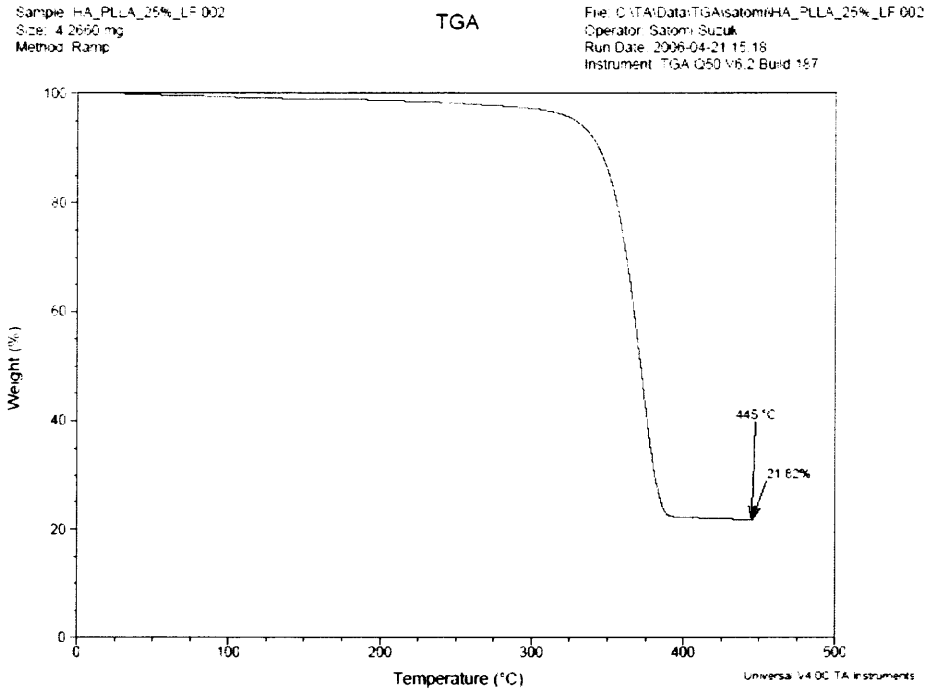

Figure B.11 Percentage weight retention of pure PLLA LF - 25% HA mat.

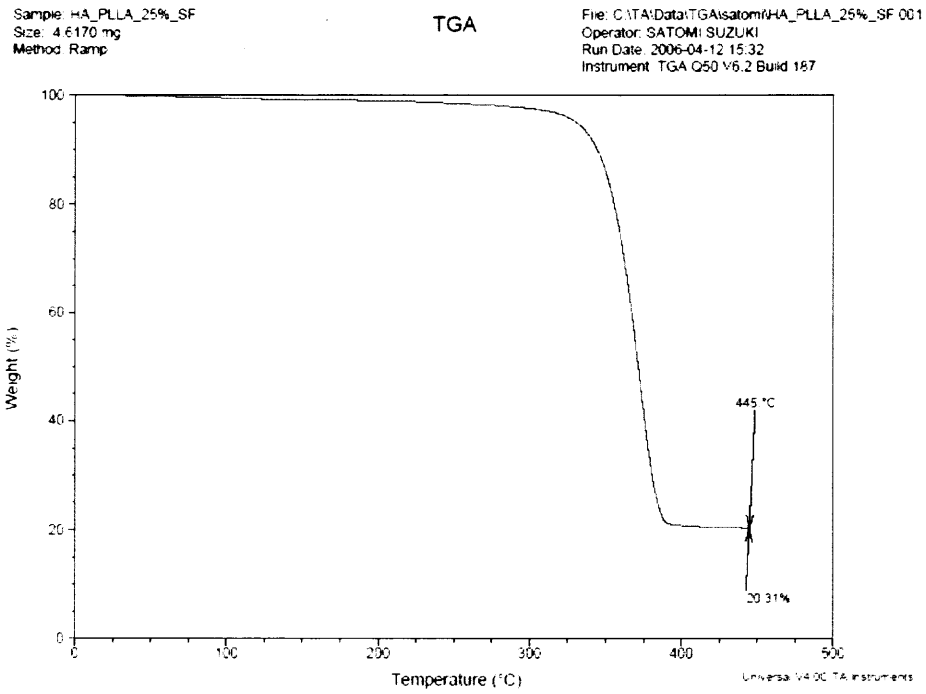

Figure B.12 Percentage weight retention of pure PLLA SF - 25% HA mat.

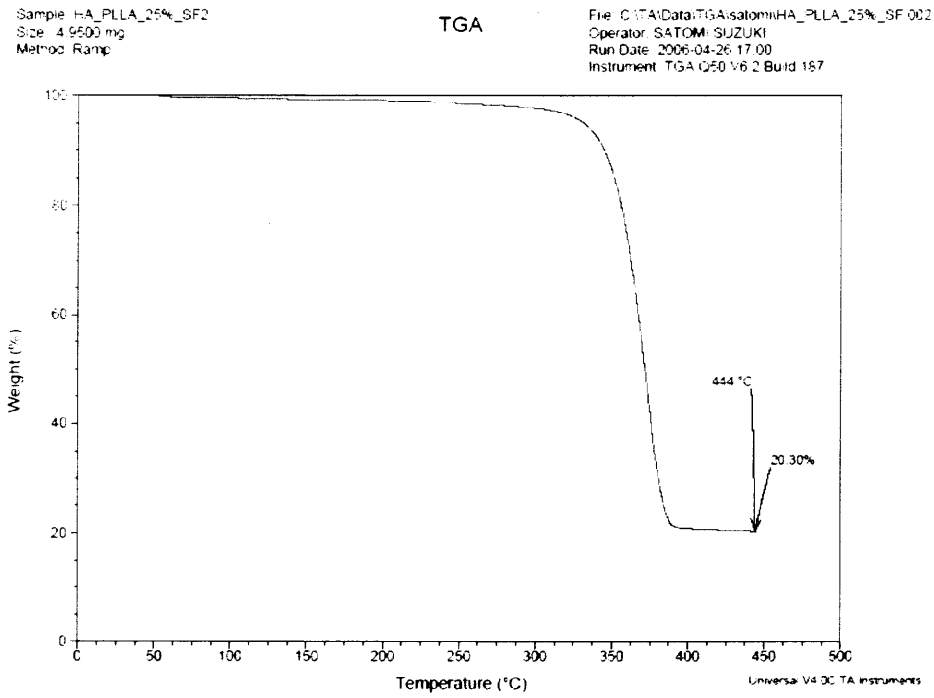

Figure B.13 Percentage weight retention of pure PLLA SF - 25% HA mat.

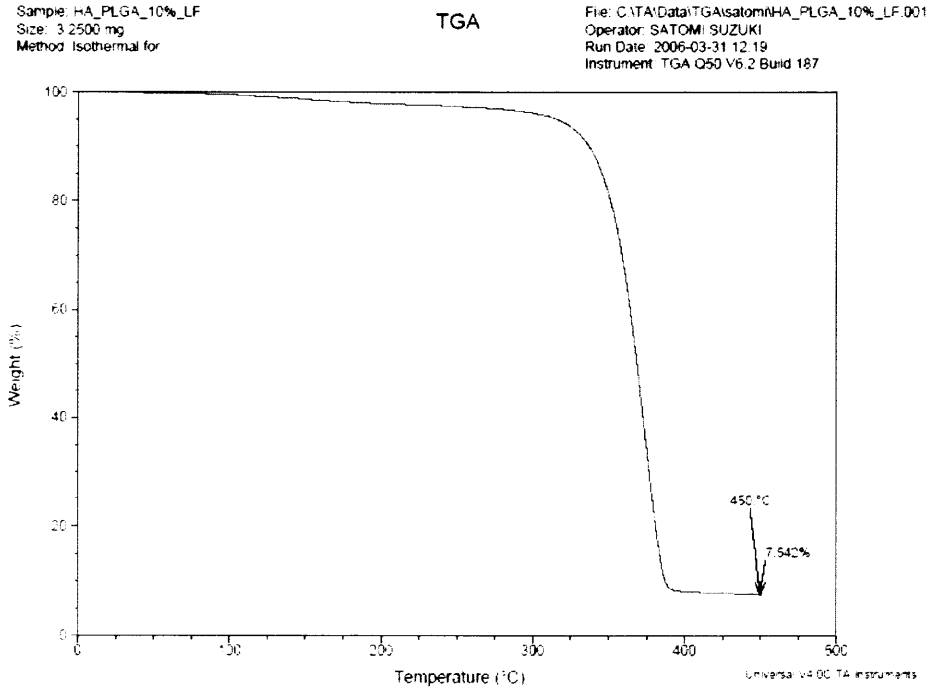

Figure B.14 Percentage weight retention of pure PLGA LF - 10% HA mat.

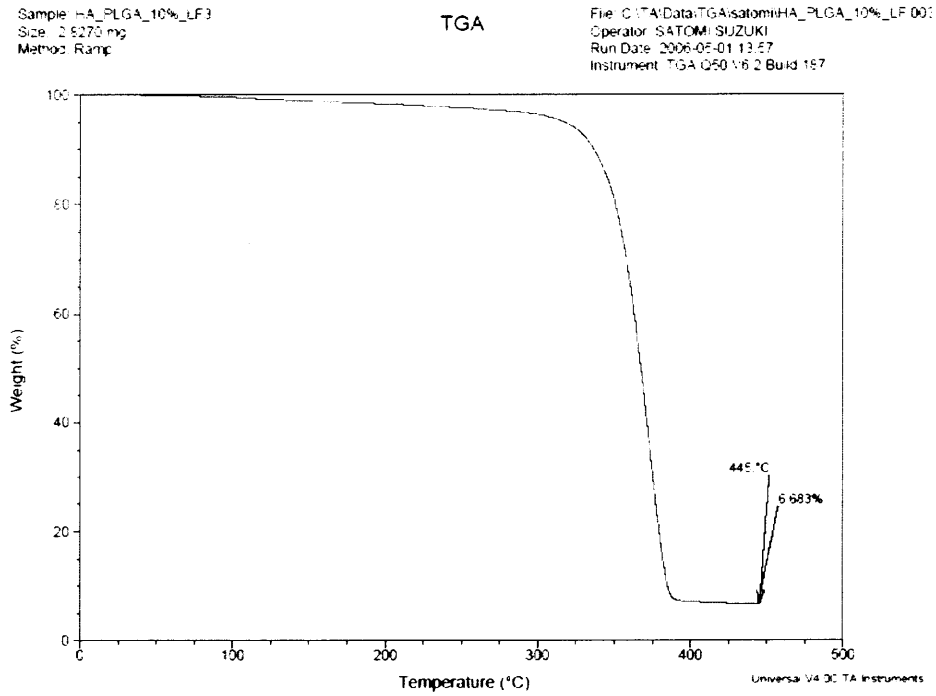

Figure B.15 Percentage weight retention of pure PLGA LF - 10% HA mat.

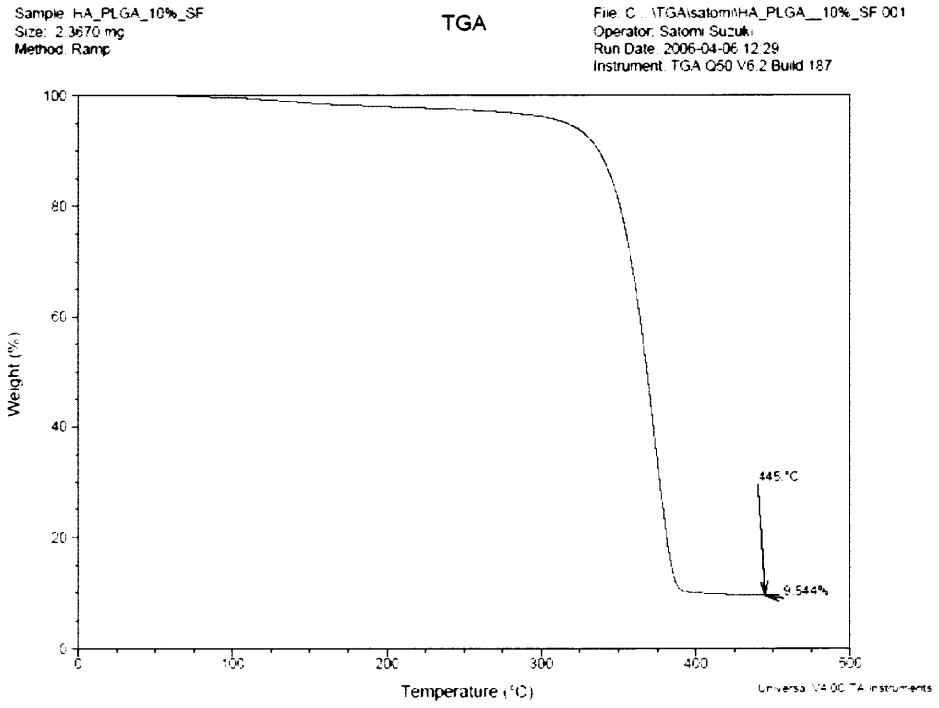

Figure B.16 Percentage weight retention of pure PLGA SF - 10% HA mat.

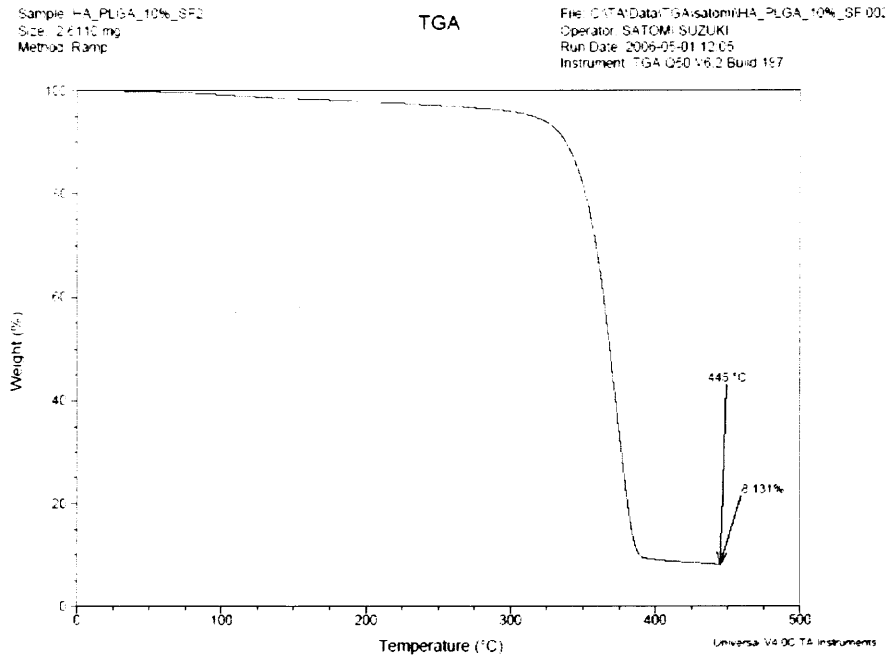

Figure B.17 Percentage weight retention of pure PLGA SF - 10% HA mat.

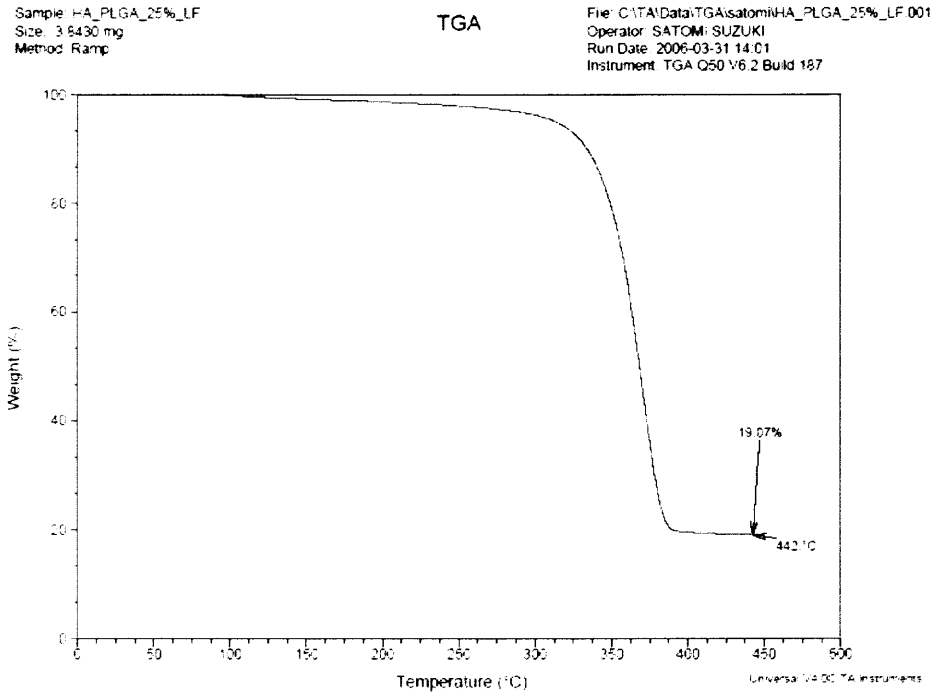

Figure B.18 Percentage weight retention of pure PLGA LF - 25% HA mat.

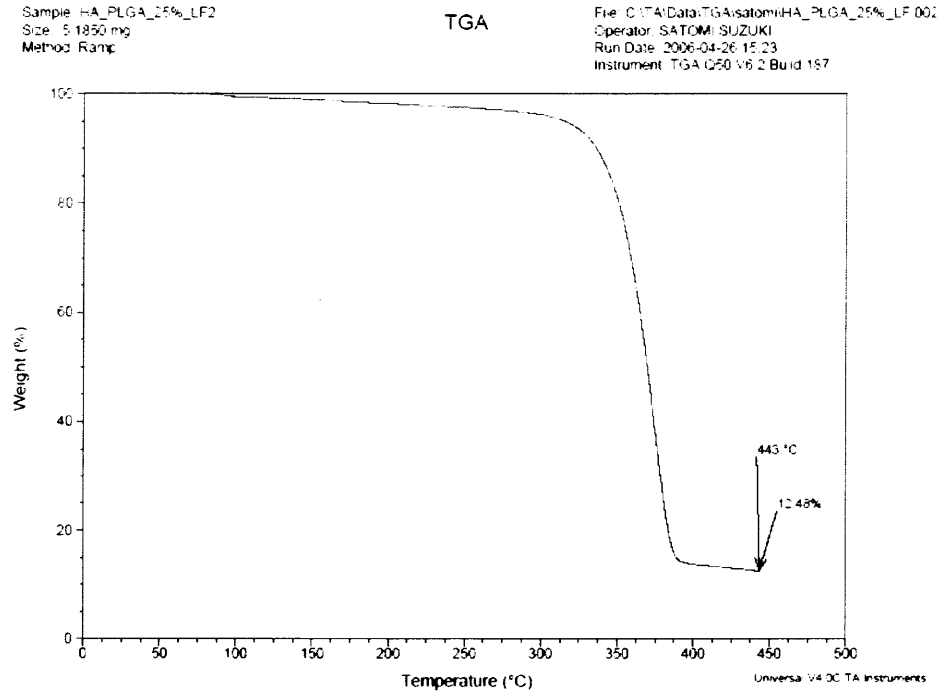

Figure B.19 Percentage weight retention of pure PLGA LF - 25% HA mat.

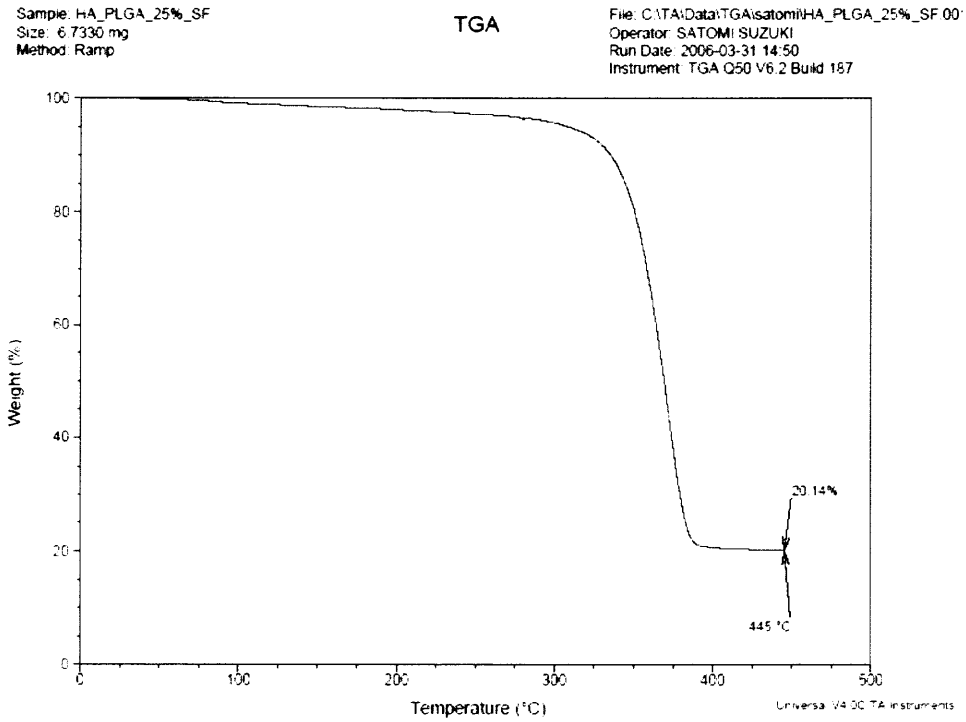

Figure B.20 Percentage weight retention of pure PLGA SF - 25% HA mat.

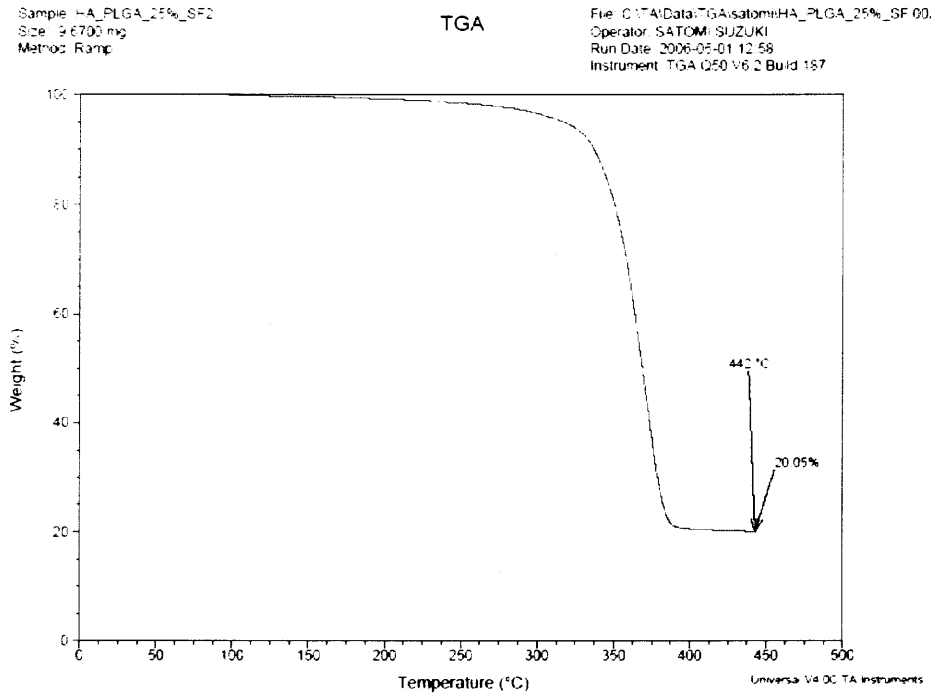

Figure B.21 Percentage weight retention of pure PLGA SF - 25% HA mat.

REFERENCES

1. Braddock, M., Houston, P., Campbell, C., Ashcroft, P. (2001). Born again bone: tissue engineering for bone repair. News Physiological Science, 16, 208-13.

2. Schrooten, Jan., Humbeeck, Jan Van., Vandessel, Wouter., Development of porous biomaterials for the healing of large bone defects [Posted on website Katholieke University, department of metallurgy and materials engineering]. Retrieved April, 2006 from the World Wide Web: http://www.mtm.kuleuven.ac.be/Research/A2P2/Biomedical.html.

3. Laurencin, Cato T., Pratt, Lillian T. (2005). The University of Virginia, Bone Graft Substitute Materials. emedicine, March 15.

4. Mastrogiacomo, M., Muraglia, A., Komlev, V., Peyrin, F., Rustichelli, F., Crovace, A., Cancedda, R. (2005) Tissue engineering of bone: search for a better scaffold. Orthodontics & Craniofacial Research, 8. 277.

5. Ma, PX., Zhang, R., Xiao, G., Franceschi, R. (2003). Engineering new bone tissue in vitro on highly porous poly(alpha-hydroxyl acids)/ hydroxyapatite composite scaffolds. Journal of Biomedical Master Res, 54. 284-93.

6. Zhang, R., Ma, PX. (1999). Porous poly(L-lactic acid)/ apatite composites created by biomimetic process. Journal of Biomedical Master Res, 45. 285-93.

7. Zhang, R., Ma, PX. (1999). Poly(alpha-hydroxyl acids)/ hydroxyapatite porous composites for bone tissue engineering. Journal of Biomedical Master Res, 44. 446-55.

8. Webster, Thomas J., Ergun, Celaletdin., Doremus, Robert H., Siegel, Richard W., Bizios, Rena. (2000). Enhanced Functions of Osteoblasts on Nanophase Ceramics. Journal of Biomaterials, 21. 1803-1810.

9. Brodie, J. C., Goldie, E., Connel, G., Merry, J., Grant, M. H. (2005). Osteoblast Interactions with Calcium Phosphate Ceramics Modified by Coating with Type I Collagen. Wiley InterScience.

10. Gittens, S. A., Uludag, H. (2001). Growth factor delivery for bone tissue engineering, J Drug Target, 9. 407-29.

11. Wei, Guobao, Ma, Peter X. (2003). Structure and properties of nano-hydroxyapatite/polymer composite scaffolds for bone tissue engineering. Biomaterials, 25. 4749-4757.

12. Formhals, A. (1934). US Patent, 1,975,504.

13. Formhals, A. (1939). US Patent, 2,160,962.

14. Formhals, A. (1940). US Patent, 2,187,306.

15. Ditzel, J. M., Kosik, W., McKnight, S. H., Beck Tan, N. C., DeSimone, J. M., Crette, S. (2002). Electrospinning of Polymer Nanofibers with Specific Surface Chemistry. polymer, 43. 1025-1029.

16. Young, John L., Fritz, April., Liu, Gonghua., Thoburn, Kathleen., Kres, Jan., Roffers, Steven. Structure of bone tissue. [Document posted on Web site Emory University]. Retrieved April, 2006 from the World Wide Web: http://training.seer.cancer.gov/module_anatomy/unit3_2_bone_tissue.html.

17. Palisson, Bernard., Bhatia, Sangeeta., Tissue Engineering, person education. 1.

18. Salgado, Antonio., Coutinho, Olga., Reis, Rui. (2004). Bone Tissue Engineering: State of the Art and Future Trends. Macromolecular Bioscience, 4. 743-765.

19. Hutmacher, D. W. (2000). Biomaterials, 21. 2259.

20. Charles N., Lane, Joseph. (1998). Current Understanding of Osteoconduction in Bone Regeneration. Clinical Orthopaedics & Related Research, 355S. 267-73.

21. Albrektsson, T., Johansson, C. (2001). Eur. Spine J., 10. S96.

22. LeGeros, R Z. (2002). Properties of osteoconductive biomaterials: calcium phosphates. Clin Orthop, 395. 81-98.

23. Yadav, Kanhaiya Lal. Hydroxyapatite Coating for Fixation of Biomedical Implants. [Document posted on Web site Indian Institute of Technology Department of Physics]. Retrieved April, 2006 from the World Wide Web: http://www.geocities.com/klyphysics/kvpy.html.

24. Nagashima, T., Ohshima, Y., Takeuchi, H. (1995). Osteoconduction in porous hydroxyapatite ceramics grafted into the defect of the lamina in experimental expansive opendoor laminoplasty in the spinal canal. Nippon Seikeigeka Gakkai Zasshi, 69. 222-30.

25. Boyde, A., Corsi, A., Quarto, R., Cancedda, R., Bianco, P. (1999). Osteoconduction in large macroporous hydroxyapatite ceramic implants: evidence for a complementary integration and disintegration mechanism. Bone, 24 (6). 579-89.

26. Yuan, H., de Bruijn, JD., Zhang, X., van Blitterswijk, CA., de Groot, K., (2001). Bone induction by porous glass ceramic made from Bioglass (45S5), J Biomed Mater Res., 58(3). 270-6.

27. Hydroxyapatite, [Document posted on Web site azom]. Retrieved April, 2006 from the World Wide Web: http://www.azom.com/details.asp?ArticleID=107.

28. Overgaard, S., Soballe, K., Lind, M., Bunger, C. (1997). Resorption of hydroxyapatite and fluorapatite coatings in man. An experimental study in trabecular bone. J Bone Joint Surg Br., 79(4). 654-9.

29. Webb, AR., Yang, J., Ameer, GA. (2004). Biodegradable polyester elastomers in tissue engineering. Expert Opin Biol Ther., 4(6). 801-12.

30. Lu, Helen H., Cooper, James Jr., Manuel, Sharron., Frreman, Joseph W., Attawia, Mohammed A., Ko, Frank K., Laurencin, Cato T. (2005). Anterior cruciate ligament regeneration using braided biodegradable scaffolds: in vitro optimization studies. Biomaterials, 26. 4805-4816.

31. Wikipedia. (2006). Polylactic acid. [Document posted on Web site Wikipedia]. Retrieved April, 2006 from the World Wide Web: http://en.wikipedia.org/wiki/Polylactic_acid.

32. Wikipedia. (2005). Polyglycolide. [Document posted on Web site Wikipedia]. Retrieved April, 2006 from the World Wide Web: http://en.wikipedia.org/wiki/Polyglycolic_acid.

33. Middleton, John C., Tipton, Arthur J. (1998). Synthetic Biodegradable Polymers as Medical Devices. Medical Plastics and Biomaterials. 30.

34. Wilkes, Garth L. (2002). Electrospinning. [Document posted on Web site Virginia Tech. Chemical Engineering Department]. Retrieved April, 2006 from the World Wide Web: http://www.che.vt.edu/Wilkes/electrospinning/electrspinning.html.

35. Yarin, A. L. Electrospinning of Nanofibers. seminar on electrospinning at the university of Illinois at Chicago.

36. Brazier-Smith, P. R., Jennings, S. G., Latham, J. (1971). An Investigation of the Behaviour of Drops and Drop-Pairs Subjected to Strong Electrical Forces. Proceedings of the Royal Society of London. Series A, Mathematical and Physical Sciences, 325. No. 1562. 363-376.

37. Yarin, A. L., Koombhongse, S., Reneker, D. H. (2001). Taylor cone and jetting from liquid droplets in electrospinning of Nanofibers, Journal of Applied Physics, 90. Issue 9. 4836-4846.

38. Murugan, R., Ramakrishna, S. (2006). Nano-featured Scaffolds for Tissue Engineering: A Review of Spinning Methodologies. Tissue Eng.

39. Kokubo, T., (1990). J.Non-Cryst. Solids, 120. 138.

40. Bharati, S., Sinha, M K., Basu, D. (2005). Hydroxyapatite coating by biomimetic method on titanium alloy using concentrated SBF. Material Science, 28. No 6. 617-621.

41. Ohtsuki, Chikara. How to prepare the simulated body fluid (SBF) and its related solutions, proposed by Kokubo and his colleagues. Nagoya University Graduate School of Engineering.

42. Anton, Rainer. Heterogeneous nucleation and growth. University of Hamburg Institute of Applied Physics.

43. Tabahashi, M., Yao, T., Kokubo, T., Minoda, M., Miyamoto, T., Nakamura, T. and Yamamuro, T. (1994). J. Am. Ceram. Soc. 77. 2805.

44. Lu, Helen H., Tang, Amy., Oh, Seong Cheol., Spalazzi, Jeffrey P., Dionisio, Kathie. (2005). Compositional Effects on the Formation of a Calcium Phosphate Layer and the Response of Osteoblast-like Cells on Polymer-bioactive Glass Composites. Biomaterials, 26. 6323-6334.

45. Causa, F., Netti, P A., Ambrosio, L., Ciapetti, G., Baldini, N., Pagani, S., Martini, D., Giunti, A. (2006). Poly-epsilon-caprolactone/hydroxyapatite composites for bone regeneration: in vitro characterization and human osteoblast response. J Biomed Mater Res A., 76(1). 151-62.

46. Laurencin, C T., Attawia, M A., Lu, L Q., Borden, M D., Lu, H H., Gorum, W J., Lieberman, JR. (2001). Poly(lactide-co-glycolide)/hydroxyapatite delivery of BMP-2-producing cells: a regional gene therapy approach to bone regeneration. Biomaterials, 22(11). 1271-7.

47. Museum of science, science learning network. SEM. [Document posted on Web site Museum of Science]. Retrieved April, 2006 from the World Wide Web: http://www.mos.org/sln/sem/.

48. MED 020 Modular High Vacuum Coating System. [Document posted on Web site Nanoscience]. Retrieved April, 2006 from the World Wide Web: http://www.nanosci.co.kr/index.htm

49. Hydroxyapatite – Hydroxyapatite Coatings An Overview. [Document posted on Web site Azom]. Retrieved April, 2006 from the World Wide Web: http://www.azom.com/details.asp?ArticleID=1405.

50. Welcome to the World of Electron Microscopy. [Document posted on Web site Iowa State University, Materials Science and Engineering Dept.]. Retrieved April, 2006 from the World Wide Web: http://mse.iastate.edu/microscopy/path2.html.

51. Köse, G. T., Tezcaner, A., Hasirci, V. (2002). Fundamentals of tissue engineering: Carrier materials and an application. Technology and Health Care, 10 (3-4). 187-201.